Petrology and geochemistry of the banded iron formation in the Eastern Sierras Pampeanas of San Luis (Argentina): implications for the evolution of the Nogolí Metamorphic Complex

Pablo D. González, Ana M. Sato, Eduardo J. Llambías, Liliane A. Petronilho

PII: S0895-9811(09)00039-X
DOI: 10.1016/j.jsames.2009.03.005
Reference: SAMES 809

To appear in: *Journal of South American Earth Sciences*

Please cite this article as: González, P.D., Sato, A.M., Llambías, E.J., Petronilho, L.A., Petrology and geochemistry of the banded iron formation in the Eastern Sierras Pampeanas of San Luis (Argentina): implications for the evolution of the Nogolí Metamorphic Complex, *Journal of South American Earth Sciences* (2009), doi: 10.1016/j.jsames.2009.03.005

Petrology and geochemistry of the banded iron formation in the Eastern Sierras Pampeanas of San Luis (Argentina): implications for the evolution of the Nogolí Metamorphic Complex

Pablo D. González[1 *], Ana M. Sato[1], Eduardo J. Llambías[1] and Liliane A. Petronilho[2]

[1] Centro de Investigaciones Geológicas (UNLP-CONICET). Calle 1 Nº. 644. B1900TAC. La Plata (Buenos Aires), Argentina.

[2] Instituto de Geociências, Universidade de São Paulo. Rua do Lago 562, CEP-05508-900. São Paulo, Brazil.

[*] Corresponding author: Tel.: +54-221-4215677 / 4258696. Fax: +54-221-4827560.

E-mail addresses: gonzapab@cig.museo.unlp.edu.ar (P.D. González); sato@cig.museo.unlp.edu.ar (A.M. Sato); llambias@cig.museo.unlp.edu.ar (E.J. Llambías); liapp@usp.br (L.A. Petronilho).

Abstract

The metamorphosed banded iron formation from the Nogolí Metamorphic Complex of western Sierra de San Luis, Eastern Sierras Pampeanas of Argentina (Nogolí area, 32°55'S – 66°15'W) is classified as an oxide facies iron formation of *Algoma Type*, with a tectonic setting possibly associated with an island arc or back arc, on the basis of field mapping, mineral and textural arrangements and whole rock geochemical features. The banded iron formation origin is mainly related to chemical precipitation of hydrogenous sediments from seawater in oceanic environments. The primary chemical precipitate is a result of solutions that represent mixtures of seawater and hydrothermal fluids, with significant dilution by mafic-ultramafic volcanic and siliciclastic materials. Multi-stage T_{DM} model ages of 1670, 1854 and 1939 Ma and positive, mantle-like $\xi Nd_{(1502)}$ values of +3.8, +1.5 and +0.5 from the banded iron formation are around the range of those mafic to ultramafic meta-volcanic rocks of Nogolí Metamorphic Complex, which are between 1679 - 1765 Ma and +2.64 to +3.68 respectively. This Sm and Nd isotopic connection suggests a close genetic relationship between ferruginous and mafic-ultramafic meta-volcanic rocks, as part of the same island arc or back arc setting. A previous Sm - Nd whole rock isochron of ~1.5 Ga performed on mafic-ultramafic meta-volcanic rocks led to the interpretation that chemical sedimentation as old as Mesoproterozoic is possible for the banded iron formation. A clockwise *P-T* path can be inferred for the regional metamorphic evolution of the

banded iron formation, with three distinctive trajectories: (1) Relict prograde M_1-M_3 segment with gradual *P* and *T* increase from greenschist facies at M_1 to amphibolite facies at M_3. (2) Peak *P-T* conditions at high amphibolite-low granulite facies during M_4. (3) Retrograde counterpart of M_4, that returns from amphibolite facies and stabilizes at greenschist facies during M_5. Each trajectory may be regarded as produced by different tectonic events related to the Pampean? (1) and the Famatinian (2 and 3) orogenies, during the Early to Middle Paleozoic. The Nogolí Metamorphic Complex is interpreted as part of a greenstone belt within the large Meso- to Neoproterozoic Pampean Terrane of the Eastern Sierras Pampeanas of Argentina.

Keywords: banded iron formation, oxide facies, Algoma Type, Sierra de San Luis, Eastern Sierras Pampeanas of Argentina.

Resumen

El mapeo de campo, la mineralogía y texturas y las características geoquímicas de roca total de la formación ferrífera bandeada metamorfizada del Complejo Metamórfico Nogolí, Sierras Pampeanas Orientales de Argentina (área de Nogolí, 32°55'S – 66°15'O) permiten clasificarla como una formación ferrífera de facies de óxidos y tipo Algoma. El ambiente tectónico se asocia posiblemente con un arco de islas o retroarco. El origen del BIF está relacionado principalmente con precipitación química de sedimentos hidrógenos desde el agua de mar en ambientes oceánicos. El precipitado químico primario es un resultado de soluciones que representan mezcla de agua de mar y fluidos hidrotermales, y significativa disolución con materiales silicoclásticos y volcánicos máfico-ultramáficos. El BIF tiene edades modelo T_{DM} de 1670, 1854 y 1939 Ma y valores mantélicos positivos de $\xi Nd_{(1502)}$ de +3.8, +1.5 y +0.5, que están en el rango de aquellos de las rocas volcánicas máficas-ultramáficas del Complejo Metamórfico Nogolí, cuyos valores varían entre 1679 - 1765 Ma y +2.64 a +3.68 respectivamente. Esta conexión isotópica Sm-Nd sugiere una estrecha vinculación genética entre las rocas volcánicas máficas-ultramáficas y las ferruginosas, como parte del mismo ambiente da arco de islas o retroarco. Una isocrona Sm-Nd roca total previa, proveniente de las rocas volcánicas máficas-ultramáficas, de ~1.5 Ga permite interpretar que para el BIF es posible una edad de sedimentación química tan antigua como Mesoproterozoico. Un patrón *P-T* horario puede ser inferido para la evolución metamórfica regional del BIF, con tres trayectorias distintivas: (1) Segmento

relíctico progrado M_1-M_3, con incremento gradual de *P* y *T* desde facies esquistos verdes en M_1 hasta facies anfibolita en M_3. (2) Pico de *P-T* en facies anfibolita alta-granulita baja durante M_4. (3) Contraparte retrógrada de M_4, que retorna desde facies anfibolita y se estabiliza en facies esquistos verdes durante M_5. Cada trayectoria puede ser vinculada con diferentes eventos tectónicos relacionados con las orogenias Pampeana? (1) y Famatiniana (2 y 3) del Paleozoico Temprano a Medio. El Complejo Metamórfico Nogolí es interpretado como parte de un *greenstone belt* dentro del Terreno Pampeano de edad meso- a neoproterozoica de las Sierras Pampeanas Orientales de Argentina.

Palabras clave: formación ferrífera bandeada, facies de óxidos, Tipo Algoma, Sierra de San Luis, Sierras Pampeanas Orientales de Argentina.

1. Introduction

Banded iron formations (BIFs) are highly controversial Precambrian chemical sedimentary rocks characterized by the presence of iron-rich layers containing at least 15% iron and commonly alternating with silica-rich layers (James, 1954; Trendall, 1983). This primary compositional layering is typically thin-bedded or finely laminated, whereas on a microscopic scale the boundary between the ferruginous and siliceous layers are distinctly sharp.

The primary layering reflects compositional differences and is preserved even when the rock is metamorphosed to high-grade conditions. The siliceous layers are composed of silica-rich material with variable crystallinity, from amorphous to microcrystalline chert, which becomes granoblastic quartz when metamorphosed. James (1954, 1966) established four distinctive facies of iron formation on the basis of predominant iron minerals within the iron-rich layers: (1) *Oxide facies,* composed of magnetite, magnetite and hematite, or hematite. Where magnetite dominates, siderite and iron silicates are usually present. (2) *Carbonate facies,* in which the most prominent carbonate minerals are siderite and ankerite. (3) *Silicate facies,* with primary iron silicate minerals and its metamorphic equivalents. (4) *Sulphide facies,* frequently formed by pyrite plus pyrrhotite mixed with siderite and other carbonates (± chert or quartz).

The classification of iron formation into *Algoma* and *Lake Superior* types was made on the basis of the contrasting conditions in the sedimentary and tectonic environments in which they have

formed (Gross, 1980, 1996). The *Algoma Type* iron formations are relatively small in size and thickness, and are associated with mafic–ultramafic to felsic volcanic or volcaniclastic rocks and greywackes in island arc - back arc regions or intracratonic rift zones. Their tectonic setting is also comparable to present day spreading ridges on the ocean floor. The *Lake Superior Type* iron formations are part of thick sedimentary units, which cover large areas of up to 10^5 km^2. This type of iron formation was deposited in relatively shallow marine environments under more stable tectonic conditions, over passive margin continental shelves. Despite the clear geological difference between the Algoma and Lake Superior types, some transitional iron formation occurrences are mentioned, especially in areas where sediments extend from continental shelf to deep-water environments.

The key aspects of BIFs related to their role in early Earth evolution, their composition, classification, temporal and spatial distribution, facies associations and depositional environment, and genesis have largely been discussed in the geological literature for nearly hundred years. Despite the major controversies involving interpretation of these features, the main geological understanding was based on well-known examples from classical greenstone belt sequences in Precambrian cratonic shields from almost all continents (Abitibi-Lake Superior, Isua, Krivoy Rog, Transvaal, Hamersley, Imataca, Quadrilátero Ferrífero and Itabira, among others; see synthesis in James and Sims, 1973; Trendall, 1983 and Huston and Logan, 2004). Less known but well documented BIFs are the Paleo? to Mesoproterozoic one in the Río de la Plata craton or Piedra Alta Terrane (Ellis, 1998) and the Neoproterozoic ones in Nico Pérez Terrane (Bossi and Navarro, 1998; Gaucher, 2000; Gaucher et al., 2003), both from Uruguay.

To the south of Uruguay, in the southernmost Río de La Plata craton at Tandilia (Argentina), banded iron formations have not been reported up to now, neither in the Paleoproterozoic basement nor in the Neoproterozoic sedimentary cover. However, recent lithological and structural mapping performed in the Eastern Sierras Pampeanas of San Luis, located to the west of Tandilia, led to the identification of a few iron-rich beds metamorphosed into high-grades, and consisting of alternating magnetite-, iron silicate- and silica-rich laminae and bands that were interpreted as an oxide facies iron formation of *Algoma Type*, with a tectonic setting possibly related to island arc or back arc regions (González, 2000, 2003, 2004). Their host rocks are high-grade rocks of the Nogolí Metamorphic

Complex, which consist of multiply deformed mafic to ultramafic and felsic volcanic rocks intercalated in psammitic to pelitic sedimentary protoliths (González et al., 2004).

In this contribution we present information on field occurrence, mineral and textural arrangements, deformational and metamorphic features of BIF from the Nogolí Metamorphic Complex of western Sierra de San Luis, Eastern Sierras Pampeanas of Argentina (Nogolí area, 32°55'S – 66°15'W, Fig. 1). The geological information is complemented with whole rock geochemical analyses, electron probe microanalytical data (EPMA) on garnets and amphiboles and a few whole rock-garnet Sm - Nd isochrons. With all these data we discuss the depositional environment and genetic relationship with coeval volcanism, the timing of sedimentation, and the age of metamorphism and deformation. Additional discussion covers the possible geotectonic context for the Nogolí Metamorphic Complex as part of the Meso- to Neoproterozoic Pampean Terrane of the Eastern Sierras Pampeanas of Argentina.

2. Geological setting

The Early Paleozoic Famatinian Orogeny of Eastern Sierras Pampeanas has been related to the accretion of the allochthonous or para-autochthonous Cuyania terrane to the southwestern Gondwana margin during the Ordovician (Ramos, 1988; Dalla Salda et al., 1992; Ramos et al., 1998; Aceñolaza et al., 2002). The tectonic and metamorphic processes related to the collision affected both the Cuyania terrane and the Gondwana autochthon, already deformed by previous orogenies, whereas the Famatinian magmatic arc was emplaced only along the autochthonous margin. Despite the intense Famatinian deformational, metamorphic and magmatic overprint, the interpretation of previous geological history assigned to the Pampean Orogeny in the Gondwana authochton is possible through a few relics of relatively well-preserved protoliths in the Nogolí Metamorphic Complex.

The high amphibolite facies rocks of the Nogolí Metamorphic Complex are considered to be the basement to the lower grade rocks (greenschist to medium amphibolite facies), represented by the San Luis Formation and Micaschist Group (Sims et al., 1998; von Gosen and Prozzi, 1998; González and Llambías, 1998). The Nogolí Metamorphic Complex is widely exposed throughout the study area, whereas the San Luis Formation and Micaschist Group crop out only as narrow strips along the eastern side of the higher-grade rocks (Fig. 1). Granitoid plutons were emplaced at different stages during the

Famatinian Orogeny, and they were classified, following the scheme presented by Llambias et al. (1998), into pre- and post-orogenic granitoids, relative to the main Famatinian deformation event that occurred during the Ordovician.

The pre-orogenic granitoids represent the arc magmatism emplaced prior to the peak Ordovician deformation and share the same penetrative Famatinian NNE-SSW to NE-SW foliation as that of the country rocks (Llambias et al., 1998). These granitoids crop out as small plutons of deformed hornblende – biotite tonalites intruded within the Nogolí Metamorphic Complex to the northwest of the study area (Fig. 1). Conventional U-Pb zircon ages of 490 to 472 Ma constrain their emplacement to the Early Ordovician (see synthesis in Sato et al., 2002, 2003a, 2004).

The El Molle and Barroso post-orogenic plutons cut the Famatinian NNE-SSW to NE-SW fabric of the Nogolí Metamorphic Complex, indicating that they intruded after the main Ordovician deformation. However, these post-orogenic plutons were later affected by reactivations of some previously developed ductile shear zones (Fig. 1). The El Molle and Barroso plutons are composed mainly of biotite – magmatic epidote (± amphibole) monzonites and amphibole – biotite – clinopyroxene diorites and gabbros, with minor two mica granodiorites and granites (González and Sato, 2000; González et al., 2006). A conventional U-Pb zircon age of 417 ± 6 ± 7 Ma constrains the El Molle pluton crystallization to Late Silurian (Sato et al., 2003 b).

2.1. Nogolí Metamorphic Complex

This unit is composed of paragneisses, micaschists, metaquartzites and migmatites, with minor orthoamphibolites, metakomatiites, komatiitic metabasalts, high-Fe tholeiite metabasalts, marbles and banded iron formation. Small lenses of two mica, garnet leucogranites of anatectic origin (now orthogneisses) are interlayered with paragneisses and migmatites. The deformation and metamorphic phase sequence was described in detail by González et al. (2004), and therefore only a brief summary is given here (Table 1).

The deformation structures of the Nogolí Metamorphic Complex were grouped into two sets with different orientations: (1) W to NW trending remnant structures attributed to pre-Famatinian (Pampean?) D_1 to D_3 phases and (2) NNE to NE trending penetrative structures related to the Famatinian D_4 and D_5 phases (González, 2003; González et al., 2004).

D_1 structures are axial plane foliation S_1 and isoclinal folds F_1 affecting compositional layering S_0 (pelite-psammite banding in paragneisses and micaschists) plus mm- to cm-thick quartz-plagioclase veins. Structures attributed to D_2 are foliation S_2, stretching lineation L_2 developed on S_2 surfaces and tight folds F_2 that refolded S_0 plus S_1 planes (and also F_1 folds). Late-D_2 and early- to syn-D_3 injection of granitic veins plus emplacement of anatectic granitoid lenses and migmatite formation are associated with ductile shear zones and their mylonitic foliation S_3 and stretching lineation L_3. Late-D_3 open folds F_3 affected the whole previous structures. Since the compositional layering S_0 is usually subparallel to S_1 and S_2, González et al. (2004) interpreted the D_1 – D_2 phases as reflecting different stages of a continuous deformation with a similar co-axial compressive regime.

Prograde regional metamorphism accompanied D_1 to D_3 deformational phases, from at least middle greenschist facies M_1 during D_1, up to the peak *P-T* conditions at high amphibolite facies M_3 contemporaneous with D_3 (Table 1).

The timing of the pre-Famatinian D_1 - M_1 to D_3 - M_3 phases is not yet well constrained by radiometric dates. This older fabric is exclusively associated with Nogolí Metamorphic Complex, and does not appear within the San Luis Formation and Micaschist Group. The U-Pb monazite age range between 520 and 490 Ma obtained on a paragneiss from the Nogolí Metamorphic Complex (González et al., 2004) is not accurate enough to assign the age of the D_1-M_1 / D_3-M_3 pre-Famatinian phases. However, we cannot rule out the effects of Mid-Cambrian Pampean Orogeny in this older fabric. The U-Pb zircon crystallization age of 507 Ma from the pre-orogenic La Escalerilla granitic pluton (von Gosen et al., 2002), which intrudes a thin strip of the Nogolí Metamorphic Complex to the southeast of our study area, also supports a pre-507 Ma tectonic and metamorphic evolution of the complex. On the other hand, the protoliths from Nogolí Metamorphic Complex, including the banded iron formation and mafic to ultramafic volcanic rocks, should be older than the D_1-M_1 to D_3-M_3 phases. Based on conventional and SHRIMP U-Pb analyses of zircon from meta-komatiite and komatiitic metabasalt, Sato et al. (2006) suggested a primary crystallization age older than 516 Ma for mafic-ultramafic volcanic protoliths of the Nogolí Metamorphic Complex, which can be as old as Mesoproterozoic time (~1.5 Ga), as shown by a previous Sm - Nd whole rock isochron (Sato et al., 2001a).

The older and multiply deformed NW-SE trending foliation was refolded and reoriented to a NNE-SSW Famatinian trend during the younger D_4 and D_5 deformational phases, and the previous high-grade metamorphoic rocks were re-metamorphosed to a new high amphibolite facies (González, 2003; González et al., 2002, 2004). The structures ascribed to D_4 phase are a foliation S_4, mineral and stretching lineation L_4 developed on S_4, and tight to isoclinal folds F_4. Several NNE-SSW trending, E or W dipping, low- to high-grade ductile shear zones also acted during D_4 and were conspicuous at D_5. This youngest deformation phase was continuous in time with D_4 and is characterized by growth and expansion of Famatinian ductile shear zones, showing S-C fabric and mylonitic foliation S_5, and reactivation of high strain zones formed in pre-Famatinian times.

The D_4 phase acted together with a medium *P* (Barrovian type) / high *T* prograde regional metamorphism M_4 which is transitional between high amphibolite- and granulite facies. A *P-T* range of ca. 8 kb and 636° to 820°C was obtained for metamorphism M_4 on both the metaclastic and mafic to ultramafic metavolcanic rocks (González, 2003; González et al., 2004). The D_5 deformational phase is ascribed to local retrograde amphibolite to greenschist facies dislocation metamorphism M_5, active only within shear zones. Away from these high strain zones, rocks of Nogolí Metamorphic Complex underwent widespread static retrograde greenschist facies metamorphism M_5, in syn- to late-D_5 conditions and in relation to the basement exhumation process.

Conventional U-Pb monazite and zircon, chemical Th-U-total Pb monazite, and Ar-Ar hornblende plateau ages from paragneisses, orthogneisses and amphibolites range between 475 and 457 Ma and constrain the timing of regional high-grade metamorphism M_4 and coeval D_4 deformation to Early to Mid-Ordovician (González et al., 2002, 2004; Sato et al., 2005, 2006). These Ordovician deformation and metamorphism, added to the granitoid arc magmatism, define the main phase of the Famatinian Orogeny in the Sierra de San Luis (Sato et al., 2002, 2003a).

The successive D_5 deformation and retrograde M_5 metamorphism are broadly constrained by K-Ar, Ar-Ar and Sm-Nd ages between 445 and 364 Ma (Ortiz Suárez, 1999; González and Sato, 2000; Sato et al., 2001b, 2002; González et al., 2004). This Late Ordovician to Late Devonian time is referred to as the late- to post-orogenic stage of Famatinian Orogeny, when post-orogenic granitoids were emplaced as well (Sato et al., 2002, 2003a).

3. Local geology of the banded iron formation

Four main beds of iron formation are intercalated with plagioclase – biotite – muscovite – quartz (± rutile) paragneisses, quartz-bearing orthoamphibolites, amphibole + orthopyroxene-rich / spinel-bearing komatiitic metabasalts and minor metachert lenses of the Nogolí Metamorphic Complex, at the top of the Barroso hill (Figs. 1 and 2). This sequence of alternating chemical plus siliciclastic sedimentary- and volcanic protoliths is included as a set of roof pendants within the post-orogenic Barroso pluton. The roof pendants together with the pluton are then cut by at least two groups of granitic dykes, some of which are depicted in Fig. 2.

The iron formations are thin lens-shaped beds 0.3 to 2 m thick and up to ~150 m long. They are boudinaged along strike and consist of fine- to medium-grained, reddish to brownish laminae and bands composed of variable amounts of iron oxides (mainly magnetite) plus minor hydroxides, iron and magnesium silicates and quartz. As magnetite is the most prominent iron-rich mineral, these ferruginous layers are classified as oxide facies iron formation.

The lamination and banding reflect the primary layering S_0 of the protolith, which is well preserved despite the regional and contact metamorphism (Figs. 3a to d). In order to avoid confusion related to the hierarchical names of layers proposed by Trendall (1965, 1983; e.g., "macro-", "meso-" or "microband"), the term band is applied in this contribution to layers thicker than 1 cm. The term lamina is used as the thinnest recognizable unit layer less than 1 cm thick, and commonly between 0.05 to 1.00 mm (Bates and Jackson, 1980). The BIF bands interbedded in Nogolí Metamorphic Complex are generally thinner than 1.3 cm (Fig. 3a), whereas the average lamina is 5.00 mm thick (Figs. 3 b to d).

The geological features described below refer to the largest bed of the iron formation (location number 1 in Fig. 1). The other layers are not treated in the text because they share the same geological features as those of the largest bed of the iron formation.

4. Deformation structures

The mesoscopic structural features of the iron formation are the same as those of the interbedded paragneisses and orthoamphibolites. The main structure attributed to D_2 is a decameter-scale tight F_2 synformal fold of the primary layering S_0 (Fig. 2). In the western limb S_0 strikes approximately N-S

and dips gently to moderately (20° - 55°) to the east (Fig. 4). The eastern limb has a NE-SW strike and a northwest dip with steeper angles (40° to 65°, Fig. 4). The F_2 fold hinge closes to the south and the fold axis plunges 24° to the NNE.

The S_1 and S_2 foliations are not well recognized within the ferruginous rocks, and this is also a common situation for other lithologies of the Nogolí Metamorphic Complex in the area (González et al., 2004). We consider that the relict foliations S_1 and S_2 are presently parallel to the penetrative S_4. Remnants of W- to WNW trending S_2 foliation, dipping between 32° and 60° to N-NNE, are poorly preserved only within meter-scale paragneiss strips at the eastern limb. Stretching and/or mineral L_2 lineation developed on S_2 is NE-plunging with low angles of 20° to 40°, and is almost parallel to the F_2 synform axis (Fig. 4). Although their parallelism might represent some relict kinematic feature related to D_2 deformation phase, it does not necessarily imply a direction of tectonic transport, in view of the fact that the iron formation layer and the hosting paragneisses are part of a roof pendant. Hence, these lineations could have been displaced, rotated or distorted during the Barroso pluton emplacement, changing their original attitude.

Several centimeter-scale parasitic tight F_2 folds are additionally found on both limbs of the large F_2 synform. Although large-scale F_1 folds are not clearly identified within the iron formation layer and paragneisses, many centimeter-scale isoclinal F_1 folds appear refolded by F_2 folds throughout the western limb.

An open to gentle F_3 or F_4 fold, ascribed to D_3 or D_4 phase and deforming S_0 plus S_1-S_2, refolded the axial trace of the F_2 synform (Fig. 2). The foliation S_4 is the penetrative planar feature in the iron formation and paragneisses; it is ascribed to the Famatinian D_4 deformation and trends NNE-SSW to NE-SW with a moderate dip (30° to 45°) to the ESE-SE (Fig. 4).

5. Petrography

The iron formation consists of alternating fine- to medium grained, reddish to brownish laminae and bands composed of magnetite, garnet, Fe-Mg clinoamphibole, apatite, minor quartz, and accessory minerals. At microscopic scale, boundaries between laminae and bands tend to be sharp, although complete gradation is also observed.

The following seven types of laminae-bands are recognized on the basis of the predominant iron-rich mineral and their textural arrangement (Fig. 5).

Type 1: Trails of idioblastic to sub-idioblastic magnetite dominate these thin (up to 3.0 mm thick) tabular or lens-shaped laminae, often accompanied by quartz either as isolated equant grains (Fig. 5a) or granoblastic polygonal aggregates. The borders of magnetite crystals are affected by martitization, which also penetrates along micro-fractures, possibly as a result of the last thermal effect related to the emplacement of the Barroso pluton (see details of metamorphism below). Apatite and garnet are distinctively absent or very scarce at the contacts with type 4 laminae, with which they alternate.

Type 2: Quartz is the main constituent of these fine-grained (<400 μm) laminae with up to 2.0 mm thickness (Fig. 5b). A typical polygonal granoblastic texture is defined by quartz with normal extinction, straight to curved boundaries and triple junctions, which suggest a late stage static recrystallization under temperature dominated conditions. Variable amounts of idioblastic apatite (5.0 mm long prisms) are accompanied by minor idioblastic to sub-idioblastic garnet and martitized magnetite. Garnet and magnetite mostly occur along contacts with type 4 laminae. Occasionally, garnet porphyroblasts show straight inclusion trails in their cores.

Type 3: are mainly composed of idioblastic garnet and interstitial quartz, with minor magnetite and apatite (Fig. 5c). The poikiloblastic garnet (up to 2.0 mm) contains quartz and magnetite inclusions homogeneously distributed from core to rim. Short rounded apatite prisms (< 0.5 mm long) appear within quartz whereas idioblastic to xenoblastic magnetite is randomly distributed among garnet grains.

Type 4: consist essentially of idioblastic to sub-idioblastic garnet and sub-idioblastic to xenoblastic magnetite, with or without quartz. Garnet is distinctively poikiloblastic, with magnetite inclusions arranged in concentric shells that alternate rhythmically with inclusion free zones (Fig. 5d). These magnetite inclusions are much smaller than matrix magnetite. From border to core in garnets, the magnetite-rich shells are distributed as follows:

- *Outer rim*: <50 μm thick, discontinuous and tabular-shaped zone, in which magnetite is arranged in a fine and dense mesh of minute crystals.

- *Inner rim*: almost continuous and up to 100 μm thick, with magnetite crystals in a looser network than the outer rim. Clots of massive magnetite may be erratically distributed around the mesh.
- *Outer core*: <100 μm thick zone consisting of an unwoven mesh of magnetite crystals that gradually becomes denser towards the core.
- *Core*: entirely composed of massive limonitized magnetite. Occasionally, some quartz grains are included within them.

Type 5: consist of massive garnet aggregates, with or without magnetite and < 1% quartz, and apatite distinctively absent (Fig. 5e). When magnetite is present it appears as a dissemination of sub-idioblastic large crystals of up to ~1.0 mm in diameter.

Type 6: are composed of seriate irregular to polygonal granoblastic garnet, inclusion-free and often accompanied by interstitial quartz, biotite, clinoamphibole, and minor xenoblastic magnetite, rutile and pyrite (Fig. 5f). Thin (<190 μm thick) intercalations of apatite lenses with polygonal granoblastic texture are conspicuous in these laminae (Fig. 5g). Some garnet crystals replace small flakes of brown biotite, and their boundaries are successively replaced by a moat of epidote or iron oxides–hydroxides. This reaction rim suggests changes in *P-T* conditions during the latest stages of the complex regional metamorphic history (see details in section 8). Clinoamphibole borders are intimately inter-grown with fine quartz and magnetite and are partly retrogressed to greenalite and crocidolite.

Type 7: are essentially dominated by sub-idioblastic clinoamphibole (belonging to the cummingtonite–grunerite series) and minor quartz, garnet, magnetite and orthoamphibole (belonging to the anthophyllite–gedrite series). Complex textural arrangements among these metamorphic minerals (including at least two generations of clinoamphiboles) represent several periods of superposed metamorphism associated with their respective deformation phases (see below). Cummingtonite–grunerite show their typical multiple twinning, and anthophyllite–gedrite are distinguished by their straight extinction (Fig. 5h). Inclusion-free sub-idioblastic garnet together with xenoblastic magnetite and quartz define the granoblastic texture of these laminae. Some clinoamphiboles are scarcely replaced by brownish patches of cryptocrystalline greenalite or bluish to greenish aggregates of crocidolite fibers. These replacement minerals are ubiquitous as moats surrounding the clinoamphibole

or growing along their cleavage. Veinlets sealed by greenalite, crocidolite, limonites and minnesotaite cut earlier mineral arrangements and are possibly related to fluid mobilization during the latest stages of regional metamorphism.

6. Mineral chemistry

Electron microprobe analyses of Fe-Mg clinoamphiboles and garnets were performed with a JEOL-SUPERPROBE JXA-8600 S electron microprobe at Instituto de Geociencias, São Paulo University. The microanalyzer includes an energy dispersive system (EDS), five wavelength dispersive spectrometers (WDS) and the Voyager-ThermoNORAN automation system with *PROZA* correction on line. The analytical conditions were: beam current of 20.10 ± 0.10 nA, acceleration voltage of 15.00 kV and a focused probe diameter of 5 μm. Natural and artificial oxides and minerals were used as standards. Na and K were counted first for 5 s to minimize loss by volatilization, and then all the other elements were counted for at least 20 s. The results were used in combination with textural information to appraise the metamorphic grades reached by the iron formation. Unfortunately, suitable mineral assemblages for quantifying the *P-T* conditions were absent in the studied rocks.

The minerals analyzed are from type 6 laminae of sample Fe-5 (see location in Fig. 2). Inclusion-free garnets and the freshest cores of the latest generation of clinoamphibole were analyzed, whereas borders of clinoamphiboles were discarded for analytical purposes because of their reaction coronas (see above). For amphibole classification the scheme of Leake et al. (1997) was followed. Selected amphibole and garnet microanalytical data are presented in Table 2.

The amphiboles are classified as monoclinic because of their oblique extinction angle. Their belonging to the Mg - Fe^{2+} - Mn^{2+} - Li member is supported by their composition, with $(Ca + Na)_B < 1$ apfu and $(Mg + Fe^{2+} + Mn^{2+} + Li)_B \geq 1$ apfu (Table 2). With Mg# (Mg/Mg + Fe^{2+}) variable between 0.50 and 0.52, and Si between 7.82 and 7.88 apfu, the amphiboles plot along the borderline between grunerite and cummingtonite, only slightly shifted towards the cummingtonite field (Table 2; Fig. 6a).

Cummingtonite is commonly found in rocks derived from regional metamorphism of Ca-poor and Fe- and Mg-rich protoliths (Deer et al., 1992), such as an iron formation. Fe and Mg replacement by Mn in these cummingtonites is generally scarce. However, under high-grade metamorphic conditions Mn content may reach up to 2 apfu in B-C sites (0.051 – 0.054 apfu for amphibolite facies

rocks, see Table 24, analyses 3 and 4, pp. 228 in Deer et al., 1992). Thus, the moderate Mn range variable between 0.1004 and 0.1060 apfu in the studied cummingtonites (Table 2) support the high-grade character of regional metamorphism that affected the iron formation.

This moderate Mn content is additionally accompanied by low Ca (0.0044 – 0.0146 apfu), Al (0.0709 – 0.1324 apfu) and alkalis (Na + K = 0.009 – 0.035 apfu), as well as a high bulk Fe# (FeO / FeO + MgO) = 0.93 (Table 4, sample Fe-5). This Ca- and Al-poor feature characterizes iron-bearing cummingtonites stable at bulk Fe# ≥ 0.40, which is another indicator of high-grade metamorphism in iron formation (Ghiorso and Evans, 2002).

The garnets are almandine rich (Xalm = 0.7376 - 0.7578), with higher content of spessartine (Xspess = 0.1202 - 0.1226) than pyrope (Xpyr = 0.1032 - 0.1115) and grossular (Xgros = 0.0174 - 0.0361), and an almost constant XFe that varies only between 0.8691 and 0.8801 (Table 2, Fig. 6b). Each individual cation content does not vary significantly between cores and rims, and this suggests that the garnet was possibly homogenized during peak metamorphic conditions. Spear (1993, and references therein) attributes this kind of homogenization to diffusion with increasing metamorphic grade, so that garnets usually reach typical almandine-rich homogeneous compositions only when attaining high amphibolite facies. According to this, the almandine-rich homogeneous composition of the studied garnet must have been acquired at peak metamorphic conditions under amphibolite facies.

The above interpretation about the metamorphic grade reached can be extended to the whole paragenesis containing equivalent cummingtonites and garnets in the iron formation from the Nogolí Metamorphic Complex. Well-documented examples related to the appearance of cummingtonite and almandine-rich garnet in high-grade metamorphosed iron formation can be found in Klein (1983).

7. Microfabrics and metamorphic evolution

For the Nogolí Metamorphic Complex, González (2003) and González et al. (2004) proposed a complex prograde Barrovian-type medium pressure / high temperature metamorphic evolution that reached granulite facies, on the basis of detailed analysis of schists, paragneisses and amphibolites (Table 1). Each metamorphic stage was linked to a coeval deformation phase. As part of the same succession, the iron formations share the same polyphase tectono-metamorphic evolution (Tables 1 and 3).

In the following sections we describe the mineral assemblages and microfabrics related to the relict pre-Famatinian M_1-D_1 to M_3-D_3 phases, those related to the Famatinian M_4-D_4 and M_5-D_5 phases, and an additional paragenesis attributable to contact metamorphism associated with the Barroso pluton, emplaced at a post-orogenic stage of the Famatinian orogeny. In addition, the *P-T* conditions of each metamorphic stage are broadly estimated using the already mentioned mineral and textural analyses. For the M_4 episode, the *P-T* approximation was additionally aided by garnet and cummingtonite compositions. Table 3 summarizes the relationship between growth periods of metamorphic minerals and deformation phases. Although this evolution might involve some loss or gain of chemical components, the regional metamorphism of the iron formation appears to be essentially isochemical, based on the remarkable consistency of their bulk chemical analyses (Table 4).

7.1. Relict pre-Famatinian M_1-D_1 to M_3-D_3 phases

The metamorphic mineral assemblages and microfabrics of the relict pre-Famatinian M_1-D_1 to M_3-D_3 phases are almost entirely overprinted by the Famatinian M_4-D_4 (peak at high amphibolite facies) and M_5-D_5 phases (retrogression at greenschist facies). However, few relicts of the former are preserved among the latter mineral assemblages or as mineral inclusion trails in garnet poikiloblasts.

The quartz + chlorite + greenalite + biotite + apatite association with granolepidoblastic texture characterizing the M_1 assemblage (Table 3) is typical of greenschist facies metamorphosed iron formation, suggesting minimum *P-T* conditions of ~350°C and low pressures (Klein, 1983). Some of these M_1 minerals may persist into medium grade assemblages (Fig. 7a) accompanying the typical M_2 magnetite + biotite + cummingtonite–grunerite$_1$ association (Table 3), which in turn has been reported elsewhere as being conspicuous at the beginning of high-grade conditions, especially together with garnets in Al_2O_3-rich bulk compositions (Klein, 1983). The S_1 foliation planes are marked by poor alignment of chlorite showing replacement moats of biotite around their cores (Fig. 7b).

An interfacial dihedral angle of almost 130° between biotite and garnet grains suggests the coexistence of prograde M_1 biotite with M_2 garnet, the biotite remaining stable at least up to an early stage of the amphibolite facies M_2 event (Fig. 7c). They are accompanied by quartz + magnetite + Fe-Mg clinoamphibole (cummingtonite–grunerite$_1$) in a granoblastic to nematoblastic arrangement, which

together characterize the relict M_2 - M_3 metamorphic episodes (Table 3). The alignment of biotite-amphibole ± magnetite marks the relict S_2 foliation planes (and possibly the subsequent S_3 planes as well, Table 3, Figs. 7c and 8a). At least two generations of clinoamphibole (cummingtonite-grunerite) are identified, an early one related to the M_2-M_3 events and a later one related to the M_4 event (see below). The early one is evidenced by syn-M_4 garnet replacement of cummingtonite-grunerite$_1$ (Fig. 8a) and by some relicts of crenulated syn-M_2/M_3 cummingtonite-grunerite$_1$ (Fig. 9e).

The formation of clinoamphibole + magnetite since M_2 possibly involved the following reaction:

$$\text{Quartz + Iron oxide / Hydroxide = Fe-Mg Clinoamphibole + Magnetite + } H_2O \quad \textbf{(1)}$$

This reaction is regarded by Floran and Papike (1978) as resulting from increasing metamorphic conditions between low- and medium grades, which might also be our case.

Relict foliations S_1 and S_2 are preserved not only throughout the matrix but also as simple to complex inclusions in garnet poikiloblasts. A few M_4 garnets overprint small flakes of M_1 chlorite (Fig. 7d) or contain simple, straight inclusion trails of M_1 biotite and apatite (Fig. 7e). The M_1 chlorite was possibly consumed by garnet that grew during prograde M_2, M_3 and subsequent peak M_4 episodes. The first garnet formation during M_2 possibly involved the following reaction, with quartz in excess:

$$\text{Chlorite + Quartz = Garnet + } H_2O \quad \textbf{(2)}$$

Within the iron formation of the Nogolí Metamorphic Complex, reactions **(1)** and **(2)** might have taken place together to form the general M_2 paragenesis of garnet + magnetite + clinoamphibole, the last mineral marking changes in metamorphic grade from the greenschist facies M_1 episode to middle-high amphibolite facies M_2-M_3 (Table 3).

Apatite may participate in mineral reaction (2), at least partly since the M_2 episode (Table 3), as the only source of grossular molecules in garnet. This interpretation is supported by large crystals of apatite showing interlobate to amoeboid grain boundaries with adjacent garnet (Fig. 7f), which

suggests some process of solid-state diffusion creep or grain boundary sliding under high grade metamorphic conditions (Passchier and Trouw, 1996), causing μm scale Ca^{2+} mobilization to form garnet contemporaneously with these deformation mechanisms. The conspicuous recrystallization of apatite during these relict metamorphic events is also denoted by inclusions of needles and short prisms within hosting garnet grains (Figs. 7e and f).

Relict grains of greenalite-iron oxide/hydroxide (possibly hematite) are additionally found as small and scarce inclusions in M_2 magnetite. The spherical granules of microcrystalline greenalite may represent replacement of relict primary oolitic sedimentary texture, preserved by armor magnetite (Fig. 7g). The irregular bleb-like shape of relict iron oxide/hydroxide included in magnetite suggests their possible primary origin as hematite-rich grain (Fig. 7h).

Complex and curved inclusion trails of quartz, apatite and magnetite in large garnet poikiloblasts also define relics of S_{1-2} foliation planes (Figs. 9a to d). This garnet growth can be interpreted as an intertectonic event (post D_{1-2} and pre- to syn-D_4) because the internal foliations S_{1-2} are oblique to the external S_4. Therefore, the garnet porphyroblasts must have grown over relict foliations S_{1-2} and then surrounded foliation S_4 that is marked by aligned quartz + magnetite + apatite + cummingtonite (Figs. 9a to d).

Some "ghosts" of tight F_{2-3} micro-fold hinges denoted by recrystallized quartz + magnetite + cummingtonite may be ascribed to polygonal arcs (Fig. 9e). This structure suggests that a relict foliation (S_1?) was progressively obliterated by recrystallization of new grains under amphibolite facies conditions (Passchier and Trouw, 1996). Isoclinal F_1 micro-folds of primary lamination S_0 (Fig. 9f) and micro-boudins with necks sealed by quartz and idioblastic magnetite (Fig. 9g) are additional pre-M_4-D_4 relict microstructures.

Assemblages containing garnet and Fe-Mg clinoamphibole, comparable to those cited for the M_2 and M_3 events, are stable in a wide range of *P-T* conditions, from 450–615°C / 2-5 kb (Floran and Papike, 1978; Haase, 1982; Klein, 1983) to 650–750°C / 4–6 kb (Immega and Klein, 1976; Ghiorso and Evans, 2002). Taking into account that biotite consumption occurs during M_2 while reaching high-grade conditions and that the magnetite + garnet + cummingtonite-grunerite$_1$ association characterizes

mainly the amphibolite facies, we estimate the ranges 650-750°C and 4-6 kb as the maximum *P-T* conditions reached by the M_3 episode, whereas the M_2 conditions must have been lower.

7.2. Peak Famatinian M_4-D_4 phase

The mineral assemblage for the peak M_4-D_4 phase is quartz + magnetite + almandine-rich garnet (Table 2) + cummingtonite (XFe 0.47 – 0.49, Table 2) + apatite ± rutile ± pyrite (Table 3). This cummingtonite represents the second generation of clinoamphibole in the iron formation. Their syn-M_4/D_4 character is indicated by alignment of tabular crystals together with garnet grains which define the S_4 foliation planes (Fig. 8a). Recrystallization and grain growth under high temperature conditions are probably the dominant factors controlling the S_4 foliation development during the M_4-D_4 phase. Continuous recrystallization of apatite during M_4-D_4 is evidenced by polygonal granoblastic grains stable with syn-M_4 garnets (Fig. 5g).

Quartz, magnetite and garnet have grown since the M_2 episode, but the recrystallization of garnet is especially ubiquitous during peak M_4 conditions under high amphibolite facies, occurring at this stage together with the almandine-rich homogenization and the Mn enrichment of cummingtonite. Small syn-M_4 garnet crystals are generally clean (with very little magnetite inclusions, Figs. 8a to c) but some large poikiloblastic crystals carry inclusions of chlorite and biotite (Figs. 7d and e) or magnetite (Figs. 9a to d) from previous metamorphic paragenesis.

The complex distribution of magnetite inclusions in garnet suggests the possibility of their inclusion in a passive manner, without significant displacement by the growing garnet since at least the M_2 episode (Table 3). As stated above, garnet might have grown at Al-Fe-Mg-Mn-rich sites replacing chlorite (and biotite) and found difficulty in replacing minerals lacking Al, such as magnetite or apatite. Since the mobility of Al ions is limited to μm-scale, the magnetite must have been randomly included, whereas some Ca ions were consumed by garnet production. Taking into account that magnetite crystals show homogeneous distribution only within the garnet from Type 3 laminae, we cannot rule out more complex growth mechanisms for garnets in other laminae, especially in those crystals where magnetite is arranged in concentric shells or curved inclusion trails.

On the other hand, the grain size of magnetite in inclusions is smaller than in the matrix. Passchier and Trouw (1996) established that this could be caused either by partial diffusion or by a

reaction involving the shapes of included magnetite grains. According to these authors, the sharp contrast in size between small inclusions and large matrix crystals of magnetite can be explained by progressive coarsening of the matrix after garnet growth as a consequence of grain boundary area reduction (static recrystallization and grain growth). This can imply a complex and long history of metamorphism and deformation phases such as those found in the iron formation of Nogolí Metamorphic Complex (Table 3).

The M_4 paragenesis with almandine-rich garnet + Mn-bearing cummingtonite + magnetite + quartz characterizes upper amphibolite facies conditions under medium pressure (Klein, 1978, 1983; Immega and Klein, 1976; Floran and Papike, 1978; Haase, 1982; Evans, 1986; Deer et al., 1992). In the system CaO-MgO-FeO-SiO_2-H_2O, assemblages containing cummingtonite yielded a precise temperature range of 660° to 740°C at 5 kb under quartz saturated and water undersaturated conditions (aH_2O = 0.5), also marked by a lack of orthopyroxene and olivine (Ghiorso et al., 1995; Ghiorso and Evans, 2002). In the system CaO-MgO-SiO_2-H_2O, Mg-Fe-Mn-rich amphiboles are stable up to 791°C and ~5 kb if bulk Ca/Ca+Mg composition is low, such as in iron formation. Above these *P-T* limits and at high Ca/Ca+Mg ratios, the Fe-Mg-Mn-rich amphiboles react to form clino- and orthopyroxene + olivine (Ghiorso and Evans, 2002). Therefore, 791°C may be regarded as the maximum temperature (at 5 kb) reached by the iron formation in the Nogolí Metamorphic Complex during the peak M_4 episode, considering their lack of pyroxenes and olivine. A lower temperature limit during M_4 can be placed at around 660°C for the same pressure. However, a peak pressure of ca. 8 kb is estimated for the iron formation on the basis of pressure values obtained by González et al. (2004) for their host rocks in connection with the maximum M_4 temperature. Therefore, a broad *P-T* range of 5-8 kb and 660-791ºC is suggested here as the possible conditions reached during the peak M_4 episode.

7.3. Retrograde Famatinian M_5-D_5 phase

The regional retrograde greenschist facies M_5 episode following the peak M_4 metamorphism is indicated by retrogression of garnet, yielding massive epidote rims (Figs. 8b and c). The grossular component in garnet might have been consumed by this replacement during basement exhumation (see below), and under presence of water. An epidote rim surrounding garnet is typical of an iron formation that underwent retrogressive metamorphism after peak *P-T* conditions (Dziggel et al., 2002). The

absence of oriented epidote defining a foliation suggests their stress-free static crystallization during the M_5-D_5 phase.

Replacement of some cummingtonite borders by secondary greenalite + minnesotaite ± crocidolite ± limonite is another texture associated with the M_5 retrogression. Their textural arrangement includes: (1) incomplete and discontinuous rims or massive aggregates of greenalite and minnesotaite; (2) scarce fiber sheaves of greenish to bluish crocidolite; and (3) red massive limonite. In addition, rare prismatic bluish riebeckite replaces scarcely some central parts of cummingtonite.

The greenalite-minnesotaite-crocidolite-limonite paragenesis is inferred as essentially related to aqueous fluid infiltration from host rocks towards the iron formation during cooling and exhumation associated with the M_5 episode. This fluid phase is also manifested by veinlets composed of the same secondary minerals that cut across the high-grade assemblages. However, we cannot rule out the possible introduction of some hydrothermal fluid in relation to the Barroso pluton emplacement.

Consumption of cummingtonite to form greenalite and minnesotaite possibly involved the following reactions (system CaO-FeO-SiO_2-H_2O) under quartz and H_2O saturation conditions (after Tracy and Frost, 1991):

3 Grunerite – Cummingtonite + 11 H_2O = 7 Greenalite + 10 Quartz **(3)**

15 Grunerite – Cummingtonite + 20 Quartz + 20 H_2O = 35 Minnesotaite **(4)**

Two reactions in the system FeO-SiO_2-H_2O-CO_2-O_2 (Tracy and Frost, 1991) can be associated with precipitation of greenalite and minnesotaite in veinlets:

2 Magnetite + 8 Quartz + 2 H_2O = 2 Minnesotaite + O_2 **(5)**

2 Magnetite + 4 Quartz + 4 H_2O = 2 Greenalite + O_2 **(6)**

Reactions (5) and (6) provide not only veinlet filling but also free oxygen, and therefore they constitute the means of increasing the fO_2 in the metamorphic system (see below).

The crocidolite forming reaction is not analyzed in detail here. However, the main issue regarding this mineral is the source of Na for its formation. The iron formation of Nogolí Metamorphic Complex shows the same low Na_2O character (see Table 4) as other BIFs of the world and therefore the occurrence of crocidolite cannot be related to the primary whole rock composition. At this point, we cannot rule out some Na mobility from the nearby igneous activity as a possible source of alkali ions during contact metamorphism.

The retrograde M_5 assemblage is characterized by greenalite + iron oxides-hydroxides + epidote + crocidolite + minnesotaite, which suggest broad greenschist facies conditions at low pressure. This retrogressive assemblage is associated with the basement exhumation process, and the cooling and decompression needs to be accompanied by high fO_2, H_2O-rich fluid infiltration.

7.4. Contact metamorphism

The intrusion of the post-orogenic Barroso pluton into the Nogolí Metamorphic Complex followed closely the peak regional M_4 metamorphic episode, and this was partially coeval with the retrograde metamorphism M_5 (González, 2003; González and Sato, 2000). Mineral paragenesis of contact metamorphism is not evident in the iron formation at hand specimen scale, but it is observed at microscopic scale as a static growth assemblage overprinting the regional metamorphic minerals. The absence of true hornfels in both the iron formation and host rocks, together with the lack of a contact aureole were interpreted by González (2003) and González and Sato (2000) as a result of the country rock still preserving the regional M_4 metamorphic conditions at the time of pluton emplacement. The addition of heat derived from the magmatic source in the contact area might have been disguised by the prevailing regional thermal conditions.

The main contact metamorphic assemblage consists of anthophyllite-gedrite + hematite (martite). The random arrangement of scarce idioblastic tabular anthophyllite-gedrite partially overprinting cummingtonite (Fig. 8d) indicates their static recrystallization under thermal dominated conditions. The Al-poor character of overprinted cummingtonite (< 0.73 % Al_2O_3, Table 2) suggests the possible predominance of anthophyllite over the Al-rich gedrite as the end member present in this new paragenesis.

Anthophyllite and cummingtonite have similar theoretical chemical compositions (see Deer et al., 1992). Thus, the crystallization of anthophyllite instead of recrystallization of cummingtonite-grunerite during contact metamorphism can related to an influx of aqueous phase or rise in fO_2, rather than critical changes in *P-T* conditions. Anthophyllite tends to be stable in hematite-rich assemblages with high bulk $Fe^{3+}/Fe^{3+} + Fe^{2+}$ compositions under medium to high-grade metamorphic conditions (Klein, 1983). This means that anthophyllite must have grown under amphibolite facies (equivalent to hornblende hornfels facies of Yardley, 1989; see Smulikowski et al., 2004) and increasing oxygen fugacity conditions. Equations **(5)** and **(6)** may have contributed to the O_2 production.

According to the textural analysis, hematite occurs typically as massive pseudomorphous aggregates replacing magnetite borders. This textural arrangement and the absence of oriented hematite following foliations indicate a stress-free static recrystallization under thermal dominated conditions (Lagoeiro, 1998; Rosière et al., 2001). The oxidation of magnetite to form hematite during contact metamorphism is an in situ transformation controlled by the level of fO_2 in the fluid phase (Lagoeiro, 1998), similar to that required for anthophyllite formation. The following reaction in the system $FeO\text{-}SiO_2\text{-}H_2O\text{-}CO_2\text{-}O_2$ (Tracy and Frost, 1991) possibly controlled the oxidation:

$$4\ \text{Magnetite} + O_2 = 6\ \text{Hematite} \quad \textbf{(7)}$$

The stabilization of hematite requires high fO_2 under the temperature range equivalent to high greenschist- and amphibolite facies (Klein, 1983; Tracy and Frost, 1991, Spear, 1993; Lagoeiro, 1998). According to Sharp (1991), magnetite grains of 1 mm are stable up to 500°C in water-rich conditions and up to 660°C in anhydrous conditions. Following this information and considering the presence of an aqueous phase during the contact metamorphism, the temperature reached by the iron formation must be higher than 500ºC, at pressures equivalent to those of the regional M_5 episode.

7.5. P-T metamorphic evolution of the BIF

On the basis of the mineral assemblage and textural analyses, complemented with microchemical data from selected amphiboles and garnets, a broad *P-T* path can be inferred for the metamorphic evolution

of the iron formation (Fig. 10). The path shows three distinctive trajectories: (1) Relict prograde M_1-M_3 segment with gradual *P* and *T* increase from greenschist facies at M_1 to amphibolite facies at M_3. (2) Prograde *P-T* path with a peak at high amphibolite-low granulite facies during M_4. (3) Retrograde counterpart of M_4 that returns from amphibolite facies and stabilizes at greenschist facies during M_5. This last segment possibly returns along a trajectory parallel to the former prograde M_1-M_3 segment (Fig. 10). The three segments thus combined show a clockwise *P-T* path. Each trajectory may be regarded as different tectonic events related to: (1) the Early Cambrian Pampean orogeny or even older cycles (e.g., Brasiliano-Pan African orogeny, von Gosen et al., 2002), and (2 and 3) the Ordovician to Devonian Famatinian orogeny. As part of the same succession, the iron formation shares the same clockwise *P-T* evolution followed by the paragneisses, micaschists, amphibolites, etc., of the Nogolí Metamorphic Complex (González, 2003).

8. Whole rock geochemical characteristics

Whole rock chemical analyses of the banded iron formation were carried out at Activation Laboratories Ltd., Ontario. Major elements and Au were determined by instrumental neutron activation analysis (INAA), while trace and rare earth elements were analyzed by inductively coupled plasma emission mass spectrometry (ICP-MS). Selected geochemical analyses from the iron formation of Nogolí Metamorphic Complex are presented in Table 4.

8.1 Major, minor and trace elements

The major oxide components are Fe_2O_3* (all iron as Fe^{3+}) and SiO_2, ranging between 42.70 - 54.50% and 30.83 – 41.94% respectively (Table 4). The abundance of these two oxides is related to the primary compositions of iron- and silica-rich protoliths and therefore their deposition must be mainly related to chemical precipitation. Other oxide contents show some variations, with Al_2O_3 ranging from 3.27 to 8.39%, CaO from 1.08 to 4.67%, MgO from 0.57 to 3.15% and MnO from 1.34 to 2.34%. TiO_2 (0.13 – 0.28%), Na_2O (0.01 – 0.05%) and K_2O (0.01-0.17%) are minor oxides whose sum does not exceed 1% (Table 4). A remarkable feature is the high value of P_2O_5 from 2.20 to 2.98% that is reflected in lenses composed almost entirely of apatite (Fig. 5g).

The Al_2O_3-SiO_2 discrimination diagram (after Wonder et al., 1988) provides some suggestions about the deposition of the San Luis BIF (Fig. 11a). The diagram shows that most of the ferruginous

rocks plot in the hydrogenous field and therefore primary chemical precipitation might come mostly from sea water, by chemical reaction between oxygen in water and dissolved Si + Fe. REE patterns of the ferruginous rocks (see below) agree with this origin from sea water. However, one sample plots on the hydrothermal metalliferous side of the diagram, suggesting that some hydrothermal input might have affected the BIF. This implies that Si + Fe might have come mostly from hydrothermal vents.

On the other hand, the positive correlation between Al_2O_3-SiO_2 suggests that the chemical sediments were possibly diluted with Al_2O_3-rich clastic or volcanic material and that the Si contribution was not only supplied by hydrothermal input, but also might have had the same source as that of Al_2O_3.

The Fe/Ti – Al/(Al+Fe+Mn) diagram (after Bostrom, 1973) is helpful to test the possible hydrothermal input into the hydrogenous sediments and their dilution with clastic or volcanic material. In this diagram, pure hydrothermal chemical sediments are enriched in Fe and Mn, whereas Al and Ti characterize the clastic or volcanic material. The diagram illustrates that the San Luis BIF plots close to modern metalliferous hydrothermal sediments and far away from modern pelagic-terrigenous sediments (Fig. 11b). Addition of Al_2O_3 to hydrogenous sediments imprinted by hydrothermal fluids decreases the Fe/Ti ratio and increases the Al content with respect to the hydrothermal elements, Fe and Mn. Thus, both the hydrothermal input and dilution with Al_2O_3 and TiO_2-rich materials were of significant importance for the protolith of the San Luis BIF.

The hydrothermal input is also supported by the high value of P_2O_5 (up to 2.98%, Table 4) and different positive inter-element correlations, such as P_2O_5 and Sb with Fe_2O_3 (Figs. 12e and f), and the Ge/Si ratio with Fe_2O_3 (Fig. 12g). Taking into account that iron formations particularly lack phosphate bearing minerals, the high P_2O_5 content might come from hydrothermal fluids. This P enrichment and also that of Sb and other cations as a result of large amount of hydrothermal input into iron formations was largely studied, discussed and corroborated (Klein and Beukes, 1993; Manikyamba and Naqvi, 1995; Lottermoser and Ashley, 2000 and references therein). The Ge/Si positive correlation with Fe_2O_3 in BIFs have been recently used as an indicator of iron source, dominantly derived from hydrothermal fluids (Hamade et al., 2003; Höll et al., 2007).

Other clues suggesting hydrothermal fluids input are high CaO / CaO + MgO ratios of 0.60 to

0.89 (sample Fe-5 is out of this range, Table 4) and some base and precious metal anomalies, such as V (167-288 ppm), Zn (30-297 ppm), Cu (56-405 ppm), Au (247-290 ppb) and Sn (17-158 ppm), among others (Fig. 12h). The high CaO / CaO + MgO (≈0.80) values were reported to be conspicuous in chemical sediments imprinted by hydrothermal fluids produced by basalt-seawater interaction close to the spreading ridge and active vents (Murray et al., 1991; Dasgupta et al., 1999). In the case of the iron formation from Nogolí Metamorphic Complex there is a genetic relationship between the ferruginous rocks and the intercalating mafic to ultramafic rocks which is supported not only by the above mentioned inter-element correlation but also by Sm and Nd isotopic data (see below).

The influence of clastic and volcanic components into the primary chemical sediment is also corroborated by positive correlations of Hf and Zr with Al_2O_3 (Figs. 12a and c) and Sc and Hf with SiO_2 (Figs. 12b and d). Within BIF worldwide, the positively correlated relationships between these trace and major elements were ascribed as mixing or dilution of clastic-volcanic material into chemical sedimentary precipitates (Horstmann and Hälbich, 1995; Manikyamba and Naqvi, 1995; Arora et al., 1995; Tsikos and Moore, 1997; Klein and Ladeira, 2000; Lottermoser and Ashley, 2000).

8.2 Rare earth elements

Shale normalized REE patterns (subscript "SN", normalized to NASC or North American Shale Composite, after Gromet et al., 1984) are consistent for all samples (Fig. 13). Ce and Eu anomalies are quantified by $Ce_{SN}/(0.5xLa_{SN} + 0.5xPr_{SN})$ and $Eu_{SN}/(0.67xSm_{SN} + 0.33xTb_{SN})$ respectively, following Bau and Dulski (1996). Yttrium is inserted between Dy and Ho according to its ionic radius because of the similar chemical behavior to those of the REE, so that they are described together (Henderson, 1984; Bau and Dulski, 1996, 1999).

The REE diagram shows a general flat pattern (La/Yb_{SN} = 0,67-1,04; Table 4), with only slight MREE (Gd to Ho) and HREE (Er to Lu) enrichment relative to LREE (La to Sm), a negative Ce anomaly (0.59-0.85) and positive Eu (1.10-2.22) and Y anomalies (Fig. 12 and Table 4). Such REE patterns and both the negative Ce and positive Y anomalies are considered chemical features inherited from interaction with seawater (Graf, 1978; Bau and Dulski, 1996, 1999; Tsikos and Moore, 1997; Klein and Ladeira, 2000, Lottermoser and Ashley, 2000, among others), and thus the REE + Y abundances in hydrogenous sediments reflect interaction with seawater. On the other hand, the

positive Eu anomaly might well result from hydrothermal input, since other elements clearly suggest a hydrothermal imprint on the BIF.

9. Sm-Nd isotopic data

In order to obtain information on the timing of the M_4 metamorphism we attempted three pairs of whole rock – garnet Sm-Nd isochrones. The whole rock samples and garnet concentrates preparation (crushing, milling and mineral separation with water-based elutriation and Frantz Isodynamic magnetic separator) were performed at the Centro de Investigaciones Geológicas, La Plata. Sm - Nd isotope dilution analyses of these materials were performed following the technique described by Sato et al. (1995) at the Centro de Pesquisas Geocronológicas (Instituto de Geociencias, São Paulo University). The Sm - Nd ages were calculated using the Isoplot/Ex version 2.49 program (Ludwig, 2001).

Selection of garnet was based on the fact that this mineral achieved major element homogenization during peak M_4 metamorphism within upper amphibolite facies conditions, with temperatures higher than 660°C, which are in the range of the closure temperature expected for garnets (Mezger et al., 1992). Locations of the samples selected, Fe-1, Fe-3 and Fe-5, are in Fig. 2, and the isotopic data in Table 5. Although strongly poikiloblastic garnets were avoided, within the separated grain size (88 to 125 μm) it was not possible to avoid tiny inclusions, mainly of magnetite, apatite and clinoamphibole. The optical assessment of impurities in garnet concentrates were less than 0.5% for Fe-5, about 1% for Fe-3 and 2% for Fe-1.

Nd contents of garnets are rather high, with 6.1 ppm (Fe-5), 6.8 ppm (Fe-3) and 14.1 ppm (Fe-1), which yield $^{147}Sm/^{144}Nd$ ratios of only 0.18, 0.20 and 0.15 respectively, with only little difference from their whole rock ratios (0.14, 0.13 and 0.12 respectively). These contents and ratios suggest that they do not represent primary garnet compositions but are most probably influenced by inclusions containing high REE, as shown by Thöni (2003), especially in the case of Fe-1. Regression lines of two-point isochrones define the following scattered dates: sample Fe-1 121 ± 100 Ma, sample Fe-3 390 ± 33 Ma, and sample Fe-5 448 ± 230 Ma (Fig. 14a to c).

All these dates are younger than the 475-457 Ma time span previously defined for the long-lasting M_4 metamorphic event that affected the paragneisses, orthogneisses and amphibolites of the

area (González et al., 2004; Sato et al., 2005, 2006). The oldest date of 448 Ma corresponds to the garnet separates least affected by inclusions and is close to the ~445 Ma determined by Ar-Ar and Sm-Nd methods and regarded as an early stage of retrogressive M_5 metamorphism related to ductile shear zones (González et al., 2004). Isotopic equilibration between garnet and inclusions might have been complete during M_4 metamorphism, and we may tentatively interpret this date as representing some post-peak, late stage of the M_4 event or an early stage of the M_5 event.

The Early Devonian date of 390 Ma (sample Fe-3) also has two possible interpretations: (1) Age of retrogressive metamorphism M_5 and ductile shearing D_5 related to the post-orogenic stage of the Famatinian orogeny, whose activity outlasted the emplacement of the post-orogenic Barroso pluton. Available K-Ar, Ar-Ar and Sm-Nd M_5-D_5 dates between 414 and 351 Ma for this stage (Sato et al., 2003b) support this interpretation. (2) Reset age produced by contact metamorphism associated with emplacement of the Barroso pluton (post-M_4-D_4 and pre- to syn-M_5-D_5). This pluton together with the El Molle pluton form a sub-circular intrusion of about 9 km by 8 km, while the iron formation and intercalating gneisses and amphibolites crop out as roof pendants within the Barroso pluton. Since 417 Ma is the U-Pb crystallization age of the El Molle pluton (Sato et al., 2003b, González et al., 2006), the date of 390 Ma may represent a cooling age after the thermal input.

The remaining date of 121 Ma defined by sample Fe-1 is considered as a spurious age, without geological meaning, because by the Late Paleozoic all tectono-thermal events had already ceased in the Sierras Pampeanas basement and the analyzed sample was the most inclusion-affected one.

Therefore, from the Sm-Nd dating, only vague constraints of post-peak-M_4 events can be derived. Despite this, and assuming that the Sm-Nd isotopic system remained undisturbed since the deposition of the BIF, we can draw some additional information from the data.

T_{DM} model ages were calculated according to DePaolo et al. (1991) for the whole-rock samples of ferruginous rocks, and they yielded 1670 Ma, 1854 Ma and 1939 Ma (samples Fe-1, Fe-3 and Fe-5 respectively, Table 5). $\xi Nd_{(t)}$ was calculated assuming a sedimentation age of the iron formation of 1502 Ma, on the basis of a Sm-Nd whole rock isochron of 1502 ± 95 Ma obtained from

mafic to ultramafic lavas intercalated with ferruginous rocks within the same sequence of the Nogolí Metamorphic Complex (Sato et al., 2001a). The calculated $\xi Nd_{(1502)}$ values are +3.8, +1.5 and +0.5.

These positive, mantle-like $\xi Nd_{(1502)}$ values are around the range of those mafic to ultramafic rocks of Nogolí Metamorphic Complex, which are between +2.64 and +3.68 (Tables 5 and 6). The T_{DM} model ages obtained are also similar to the 1679 to 1765 Ma range for the mafic to ultramafic rocks (Tables 5 and 6), with slightly higher values. However, an additional comparison of $^{147}Sm/^{143}Nd$ ratios indicates that the 0.124 to 0.136 range for the ferruginous rocks are lower and more fractionated than the near chondritic range of 0.158 to 0.193 for the mafic to ultramafic rocks.

10. Origin and tectonic setting of the banded iron formation

The lamination and banding of the iron formation reflect their primary compositional layering S_0 and therefore the origin of their protolith must be related mainly to chemical precipitation of hydrogenous sediments from seawater in oceanic environments. Predominance of magnetite allows the classification of the BIF as oxide facies iron formation. Alternating iron-rich (Type 1) and silica-rich (Type 2) laminae and bands would reflect cyclic changes in seawater chemical parameters, such as pH, Eh and ion concentrations.

The remarkable consistency of the bulk compositions suggests that despite the high-grade metamorphism and poly-deformational history of the San Luis BIF, some primary depositional features and major oxide, trace and rare earth element compositions of their protolith are basically preserved, and therefore could represent the primary composition of hydrogenous sediments. Klein (1973) compared several chemical analyses of iron formation affected by low- to high-grade metamorphism and concluded that apart from the loss of volatiles, particularly CO_2 and H_2O, major element oxide concentrations do not appear significantly affected by regional metamorphism. Effects of metamorphism on the REE distribution in iron formation have been found to be only of minor importance in most cases (Bau and Dulski, 1996) or directly the REE were also directly considered immobile (Bingen et al., 1996).

Major and minor oxide and inter-element ratios in iron formation are complex because chemical precipitates commonly reflect contributions of several sources, including seawater, volcanic and clastic material and hydrothermal fluids (Hatton and Davidson, 2004 and references therein). In

the case of the San Luis banded iron formation, the geochemical signature of the primary chemical precipitates represents mixtures of seawater and hydrothermal fluids, with significant participation of mafic-ultramafic volcanic and clastic materials.

The seawater inheritance can be recognized from the almost flat REE pattern (La/Yb_{SN} = 0.67-1.04), with a slight LREE depletion and HREE enrichment, negative Ce plus positive Y anomalies. The hydrothermal imprint can be traced through enrichment of Si, Fe, P, Ca, Mg, metals (V, Zn, Co, Cu, Au, among others), in addition to a positive Eu anomaly. The temperature of these hydrothermal fluids is difficult to assess. However, some inference can be made using Eu_{CN} values (subscript "CN" refers to chondrite normalized after Nakamura, 1974). According to Bau and Dulski (1996, 1999), values of $Eu_{CN} \approx 1$ characterize low temperature hydrothermal fluids (< 250°C), whereas highly pronounced positive Eu_{CN} anomalies are typical of high temperature (> 350°C) present day black smoker solutions. These chemical features of Eu_{CN} are not ubiquitous in the ferruginous rocks treated here, and therefore on the basis of $Eu_{CN} > 1$ [$(Eu/Eu^*)_{CN}$ = 1.33-2.85, Table 4] we suggest a range of moderate temperature variable between 250° and 350°C for the hydrothermal fluids that contributed to the bulk chemistry of the San Luis BIF.

Al-Ti (and other cations such us Zr, Hf, Sc ± Si) might come from contemporaneous volcanic and clastic protoliths of the Nogolí Metamorphic Complex. This is illustrated in the Fe/Ti – Al/(Al+Fe+Mn) diagram (Fig. 11b) by a "mixing curve", upon which the ferruginous rocks are plotted towards the hydrothermal-rich side, while the paragneisses and micaschists from the same complex are on the clastic side, and the meta-komatiites, komatiitc meta-basalts and high-Fe tholeiite meta-basalts are midway between the two extremes. The mafic to ultramafic rocks appear to be the main contaminant for the pure chemical sediment of the iron formation, whereas felsic volcanic rocks and pelites-psammites appear as less important.

Precambrian iron formations around the world free from clastic contaminators display similar REE signatures, with $(Sm/Yb)_{SN} < 1$, $(Eu/Sm)_{SN} > 1$ and $(La/Sm)_{CN} > 1$ (Bau and Dulski, 1996 and references therein). In the studied ferruginous rocks, the ranges of these ratios are $(Sm/Yb)_{SN}$ 0.67 - 0.89, $(Eu/Sm)_{SN}$ 1.24 - 2.34, and $(La/Sm)_{CN}$ 0.62 – 0.72 (Table 4). Although the ratio $(La/Sm)_{CN} < 1$ may indicate volcanic and clastic contamination, the first two ratios are in good agreement with those

from iron formations around the world, suggesting that the volcanic-clastic contribution could have been only of relative importance.

The genetic relationship between ferruginous and mafic-ultramafic volcanic rocks is further corroborated by Sm and Nd isotopic data. The interaction between solutions related to chemical precipitation (mixtures of seawater and hydrothermal fluids) and mafic-ultramafic volcanism can be traced by the mantle-like positive ξNd (t) of ferruginous rocks (see section 9). Many authors, such as Jacobsen and Pimentel-Klose (1988), Alibert and McCulloch (1993), Bau et al. (1997) and Frei et al. (1999), have modeled the influence of hydrothermal circulation of seawater through mid-ocean ridge basalts during the formation of banded iron formation on the basis of Nd isotopic characterization. Following their arguments, we suggest that although the seawater from which the San Luis BIF precipitated shows clear hydrothermal influence from the mafic to ultramafic rocks (positive ξNd values and the similar T_{DM} ages), a pre-existing continental component cannot be denied because of the fractionated $^{147}Sm/^{143}Nd$ ratios and some very slightly older T_{DM} ages. Both components are consistent with those detected through the major, trace and whole REE analyses.

Small size, scarce distribution, association with volcanic rocks, geochemical signature, some metal contents (Cu, V, Zn, Co, among others), and Sm-Nd isotopic data characterize the San Luis BIF as an *Algoma Type* iron formation. The Sc content is lower than that of typical *Algoma* type and closer to that of *Lake Superior* type iron formation, in which clastic sedimentary rocks predominate over volcanic successions (Fig. 12h). Therefore, this situation favors the idea of contamination by volcanic and clastic components, as previously stated by major elements.

Island arc or back arc regions are the possible tectonic setting of the banded iron formation, where they are intercalated with mafic to ultramafic rocks. This interpretation is supported by: (1) Major, trace and rare earth element composition of the mafic to ultramafic rocks, consistent with island arc tholeiites or MORB-like basalts of spreading ridge centers (González et al., 2002; González, 2003). (2) The main contaminant of the primary chemical hydrogenous sediment is mafic to ultramafic volcanism, with minor contributions of felsic volcanism, pelites and psammites. The significant importance of the volcanic contribution leads to the interpretation that the banded iron formation was deposited in a volcanic island arc setting or close to it. (3) Mantle-like positive ξNd (t) values of the

mafic-ultramafic rocks ranging between +2.64 and +3.68 (Table 6) are consistent with a primitive island arc or back arc origin (Dickin, 1995), and (4) Mantle-like positive ξNd (t) and Paleoproterozoic T_{DM} model ages of ferruginous rocks, as a result of hydrothermal circulation associated with mafic to ultramafic volcanic rocks (Jacobsen and Pimentel-Klose (1988).

11. Temporal constraints of the BIF and evolution of the Nogolí Metamorphic Complex

Banded iron formations are usually void of suitable minerals to apply direct isotopic datings (e.g., zircon or monazite for U-Pb method) and for this reason many of them are ambiguous in age. For several BIFs, a synchronous age with associated volcanic rocks has been assumed (James, 1983; Chemale et al., 1994, among others). The sedimentation of the San Luis banded iron formation might be as old as Mesoproterozoic (~1.5 Ga), on the basis of a Sm-Nd whole rock isochron of coeval mafic to ultramafic volcanism (Sato et al., 2001a).

If the Mesoproterozoic age of the banded iron formation and mafic to ultramafic meta-volcanic rocks was correct, then it would be reasonable to assume a Precambrian age for the whole Nogolí Metamorphic Complex. Further Precambrian age constraints are: (1) A U-Pb zircon crystallization age of 507 Ma from the La Escalerilla pluton (von Gosen et al., 2002), which intrudes a thin strip of the complex to the southeast of our study area. (2) Conventional and SHRIMP U-Pb zircon data from meta-komatiite and komatiitic metabasalt. Based on these data, Sato et al. (2006) suggested a primary magmatic crystallization age older than 516 Ma for the extrusion of komatiitic to basaltic lava flows, and (3) The preliminary U-Pb zircon age of 554 ± 5 Ma for a feldspar biotite gneiss from the complex, interpreted as the crystallization age of the gneiss (Vujovich and Ostera, 2003). These U-Pb ages suggest a pre-Early Cambrian timing of sedimentation, metamorphism and deformation (M_1-D_1 to M_3-D_3 events) for the relict pre-Famatinian geological history of the Nogolí Metamorphic Complex.

The Sm-Nd dating of ferruginous rocks were not appropriate to constrain the timing of peak M_4 tectono-metamorphic conditions, and it gave only imprecise indications for the post-M_4 events. However, it is reasonable to assume an Early to Middle Ordovician age (between 475 and 457 Ma) as the timing of regional high-grade metamorphism M_4 and the coeval D_4 deformation, according to the ages presented by González et al. (2002, 2004) and Sato et al. (2005, 2006) from paragneisses,

orthogneisses and amphibolites intercalated in the Nogolí Metamorphic Complex. The 448 Ma and 390 Ma Sm-Nd isochron ages obtained in this contribution from ferruginous rocks allow a broad estimation of the M_5 event as post-457 Ma, within Silurian to Devonian times.

The association of banded iron formation with komatiitic volcanic rocks and Ba-Ca exhalites described in González et al. (2005) make up a peculiar rock group within the Nogolí Metamorphic Complex of the western Sierras de San Luis. Up to now, no other comparable rocks or association have been reported in the surrounding area of the Sierra de San Luis or the entire Eastern Sierras Pampeanas. They are protoliths typically found in supracrustal successions of greenstone belts, in Precambrian cratonic shields from almost all continents (Condie, 1997; Huston and Logan, 2004). Therefore, it appears reasonable to consider the Nogoli Metamorphic Complex as having been part of a Precambrian greenstone belt, later affected by polyphase deformation and regional high-grade metamorphism during Early Paleozoic Pampean and Famatinian orogenies. The ca. 1.5 Ga age of the banded iron formation and mafic to ultramafic volcanic rocks may suggest a Mesoproterozoic timing of formation for this greenstone belt in Eastern Sierras Pampeanas.

Greenstone belts can be equated to a terrane, and more specifically to an oceanic terrane (Condie, 1997). Following this idea, we suggest that the Nogolí Metamorphic Complex might represent a small piece (island arc-back arc setting?) of a larger terrane, such as the previously envisaged Pampean- (Ramos, 1988) or Pampia Terrane (Ramos and Vujovich, 1993a). This terrane was originally proposed as comprising Meso- to Neoproterozoic basement rocks, partially overlapping the blocks of the Eastern Sierras Pampeanas of Argentina (Ramos and Vujovich, 1993b).

It is noteworthy that island arc to back arc settings were formerly proposed by Ramos (1991) for all the mafic-ultramafic exposures of the Sierras de San Luis, including the meta-volcanic rocks of the Nogolí Metamorphic Complex. At least two island arcs were considered by Ramos (1991) as developing during Meso- to Neoproterozoic times, and later colliding against the western margin of the Río de la Plata craton. This would suggest that Pampean Terrane could represent a protracted island arc-back arc system developed to the west of the Río de la Plata craton, as part of the Western Gondwana supercontinent (see, e.g. Unrug, 1996; Brito Neves et al., 1999).

We are carrying out new geochronological, geochemical and isotopic studies on several protoliths of the Nogolí Metamorphic Complex to better define their age, whole rock compositional features, extension in the Sierras de San Luis and correlation with other basement blocks from Eastern Sierras Pampeanas. All these data will provide not only more accurate evidences for the Precambrian evolution of the Nogolí Metamorphic Complex, but also supply a better understanding of their geotectonic context as part of the Pampean Terrane in this segment of the western Gondwana margin.

12. Conclusions

The petrologic, geochemical and isotopic data of the banded iron formation from the Nogolí Metamorphic Complex of San Luis, combined with structural analyses, allow the delineation of the following conclusions:

(1) The origin of the oxide facies *Algoma Type* banded iron formation is related to primary chemical precipitation of hydrogenous sediments from seawater in oceanic environments. The geochemical signature of the hydrogenous sediments represents mixtures of seawater, hydrothermal fluids and mafic-ultramafic volcanic sources, with a minor contribution of felsic volcanism and clastic materials. The most likely setting in which the banded iron formation was deposited is an island arc to back arc region, influenced by mafic to ultramafic volcanic flows.

(2) The banded iron formation and mafic–ultramafic volcanic rocks share similar mantle-like positive ξNd (t) values and Paleoproterozoic T_{DM} model ages. These rocks have synchronous timing of formation, which may be as old as Mesoproterozoic (ca. 1.5 Ga).

(3) At least five stages of deformation under medium- to high-grade regional metamorphism affected the banded iron formation. The pre-Famatinian tectonic and metamorphic evolution (D_1-M_1 to D_3-M_3) can be related to the Early Cambrian Pampean orogeny or even older cycles (e.g. Brasiliano-Pan African orogeny, von Gosen et al., 2002), whereas the Famatinian D_4-M_4 and D_5-M_5 events can be respectively ascribed to Early to Middle Ordovician and Devonian times.

(4) The Nogolí Metamorphic Complex is a volcano-dominated supracrustal succession, in which the intercalating ferruginous-, mafic to ultramafic volcanic rocks and exhalites are unique protoliths in western Sierras de San Luis. This rock association suggests a greenstone type model for the genesis of the whole Nogolí Metamorphic Complex.

(5) The Nogolí Metamorphic Complex is interpreted as part of the large Meso- to Neoproterozoic Pampean Terrane of the Eastern Sierras Pampeanas of Argentina. After its deposition, the polyphase deformation and regional metamorphism constrained to the Early Paleozoic might have taken place in relation to complex terrane amalgamation processes along the western Gondwana margin.

Acknowledgements

We wish to thank A. Ortiz Suárez, C. Costa and A. Carugno Duran for all the aid and assistance during our days in the Departamento de Geología (Univesidad Nacional de San Luis). J. M. Ponce helped us during the fieldtrip mapping of ferruginous rocks. We are grateful to Silvio R.F. Vlach (Instituto de Geociências, Universidade de São Paulo, Brazil) for the electron microprobe analyses on minerals and to those colleagues at laboratories of CPGeo and Electron Microprobe of the same Institute, who helped us with technical assistance. We are also grateful to R.A.J. Trouw, who improved our microtectonic knowledge of ferruginous rocks under the microscope during scholarly work of P.D. González at UFRJ (Río de Janeiro, Brazil). Reviews by R. Giacosa, W. von Gosen and an anonymous referee improved the manuscript and are gratefully acknowledged. Our work within the western Sierra de San Luis was possible with the financial support of the projects 11/N435 and N528 from Facultad de Ciencias Naturales y Museo (Universidad Nacional de La Plata) and PIP 5855 from CONICET (Argentina). The satellite images were provided by CONAE (Comisión Nacional de Actividades Espaciales) of Argentina.

References

Aceñolaza, F., Miller, H., Toselli, A., 2002. Proterozoic-early Paleozoic evolution in western South America: a discussion. Tectonophysics 354, 121-137.

Alibert, C., McCulloch, M., 1993. Rare-earth elements and neodymium isotopic compositions of the banded iron-formations and associated shales from Hamersley, western Australia. Geochimica et Cosmochimica Acta 57, 187-204.

Arora, M., Govil, P., Charan, S., Uday Raj, B., Balaram, V., Manikyamba, C., Chatterjee A., Naqvi, S., 1995. Geochemistry and origin of Archaean Banded Iron Formation from Bababudan Belt, India. Economic Geology 90, 2040-2057.

Bau, M., Dulski, P., 1996. Distribution of yttrium and rare-earth elements in the Penge and Kuruman iron-formations, Transvaal Supergroup, South Africa. Precambrian Research 79, 37-55.

Bau, M., Dulski, P., 1999. Comparing yttrium and rare-earth in hydrothermal fluids from the Mid-Atlantic Ridge: implications for Y and REE behaviour during near-vent mixing and for the Y/Ho ratio of Proterozoic seawater. Chemical Geology 155, 77-90.

Bau, M., Höhndorf, A., Dulski, P., Beukes, N., 1997. Sources of rare-earth elements and iron in Paleoproterozoic iron-formations from the Transvaal Supergroup, South Africa: evidence from neodymium isotopes. Journal of Geology 105, 121-129.

Bates, R., Jackson, J., 1980. Glossary of Geology. 2nd Edition. American Geological Institute, Falls Church, Virginia, US, 749 p.

Bingen, B., Demaiffe, D., Hergoten, J., 1996. Redistribution of REE, thorium and uranium over accessory minerals in the course of amphibolite to granulite facies metamorphism: the role of apatite and monazite in orthogneisses from south-easthern Norway. Geochimica et Cosmochimica Acta 60, 1341-1354.

Bostrom, K., 1973. The origin and fate of ferromanganoan active ridge sediments. Stockholm Contribution of Geology 27, 149-243.

Bossi, J., Navarro, R., 1998. Las formaciones ferríferas de Uruguay: su significado económico y tectono-estratigráfico. 10º Congreso Latinoamericano de Geología y 4º Congreso Nacional de Geología Económica 3, 3-7.

Brito Neves, B., Campos Neto, M., Fuck, R., 1999. From Rodinia to Western Gondwana: an approach to the Brasiliano-Pan African Cycle and orogenic collage. Episodes 22 (3), 155-166.

Condie, K., 1997. Plate tectonics and crustal evolution. 4th Edition. Butterworth Heinemann, Oxford, UK, 288 p.

Chemale Jr., F., Rosière, C.A., Endo, I., 1994. The tectonic evolution of the Quadrilátero Ferrífero, Minas Gerais. Precambrian Research 65, 25–54.

Dalla Salda, L., Cingolani, C., Varela, R., 1992. Early Paleozoic orogenic belt of the Andes in the southwestern South America: Result of Laurentia-Gondwana collision? Geology 20, 617-620.

Dasgupta, H., Sambasiva Rao, V., Krishna, C., 1999. Chemical environments of deposition of ancient iron- and manganese-rich sediments and cherts. Sedimentary Geology 125, 83-98.

Deer, W., Howie R., Zussman, J., 1992. The Rock Forming Minerals. Longman Scientific & Technical. Harlow, UK, 696 p.

DePaolo, D., Linn, A., Schubert, G., 1991. The continental crust age distributions; methods of determining mantle separation ages from Sm-Nd isotopic data and application to the Southwestern United States. Journal of Geophysical Research 96 (B2), 2071-2088.

Dickin, A., 1995. Radiogenic isotope geology. Cambridge University Press. Cambridge, 490 p.

Dziggel, A., Stevens, G., Poujol, M., Anhaeusser, C., Armstrong, R., 2002. Metamorphism of the granite-greenstone terrane south of the Barberton greenstone belt, South Africa: an insight into the tectono-thermal evolution of the "lower" portions of the Onverwacht Group. Precambrian Research 114, 221-247.

Ellis, J.H., 1998. The Precambrian supracrustal rocks of the Isla Cristalina de Rivera in northern Uruguay and their ore deposits. Heidelberger Geowissenschaftliche Abhandlungen 90, 1-196.

Evans, B., 1986. Reactions among sodic, calcic and ferromagnesian amphiboles, sodic pyroxene and deerite in high-pressure metamorphosed ironstone, Siphnos, Greece. American Mineralogist 71, 1118-1125.

Floran, R., Papike, J., 1978. Mineralogy and petrology of the Gunflint Iron Formation, Minnesota-Ontario: correlation of compositional and assemblage variations at low to moderate grade. Journal of Petrology 19 (2), 215-288.

Frei, R., Bridgwater, D., Rosing, M., Stecher, O., 1999. Controversial Pb-Pb and Sm-Nd isotope results in the Archean Isua (West Greenland) oxide iron formation: Preservation of primary signatures versus secondary disturbances. Geochimica et Cosmochimica Acta 63 (3-4), 473-488.

Gaucher, C., 2000. Sedimentology, palaeontology and stratigraphy of the Arroyo del Soldado Group (Vendian to Cambrian, Uruguay). Beringeria 26, 1–120.

Gaucher, C., Boggiani, P., Sprechmann, P., Sial, A., Fairchild, T., 2003. Integrated correlation of the Vendian to Cambrian Arroyo del Soldado and Corumbá Groups (Uruguay and Brazil): palaeogeographic, palaeoclimatic and palaeobiologic implications. Precambrian Research 120 (3-4), 241-278.

Ghiorso, M., Evans, B., 2002. Thermodynamics of the amphibolites: Ca-Mg-Fe^{2+} quadrilateral. American Mineralogist 87, 79-98.

Ghiorso, M., Evans, B., Hirschmann, M., Yang, H., 1995. Thermodynamics of the amphiboles: Fe-Mg cummingtonite solid solutions. American Mineralogist 80, 502-519.

González, P.D., 2000. Banded iron formation del basamento Pre-Famatiniano de San Luis: primer registro en Argentina. In: Schalamuk, I., Brodtkorb, M., Etcheverry, R. (Eds.), Mineralogía y Metalogenia 2000. Instituto de Recursos Minerales, La Plata. Publicación N° 6, 191-198.

González, P.D., 2003. Estructura, metamorfismo y petrología del basamento ígneo-metamórfico de la Sierra de San Luis entre Nogolí y Gasparillo. Ph.D. Thesis 817 (Unpublished). Facultad de Ciencias Naturales y Museo (Universidad Nacional de La Plata), pp. 446.

González, P.D., 2004. Origin and economic potenctial of a BIF–komatiite association of the Sierras Pampeanas of Argentina. In: Muhling, J., Goldfarb, R., Vielreicher, N., Bierlein, F., Stumpfl, E., Groves, D., Kenworthy, S. (Eds.), Predictive Mineral Discovery Under Cover. Perth, Western Australia. 2004 Society of Exploration Geophysicists Conference, pp. 421.

González, P.D., Llambías, E., 1998. Estructura interna de las metamorfitas pre-Famatinianas y su relación con la deformación del Paleozoico inferior en el área de Gasparillo, San Luis, Argentina. 10° Congreso Latinoamericano de Geología y 6° Congreso Nacional de Geología Económica 2, 421-426.

González, P.D., Sato, A.M., 2000. Los plutones monzoníticos cizallados El Molle y Barroso: dos nuevos intrusivos pos-orogénicos en el oeste de las sierras de San Luis, Argentina. 9° Congreso Geológico Chileno 1 (sesión temática 4), 621-625.

González, P.D., Sato, A.M., Basei, M.A., Vlach, S.R., Llambías, E., 2002. Structure, metamorphism and age of the Pampean-Famatinian Orogenies in the western Sierra de San Luis. 15° Congreso Geológico Argentino 2, 51-56.

González, P.D., Sato, A., Llambías, E., Basei, M., Vlach, S., 2004. Early Paleozoic structural and metamorphic evolution of western Sierra de San Luis (Argentina), in relation to Cuyania accretion. Gondwana Research 7 (4), 1157-1170.

González, P.D., Sato, A.M., Llambías, E., Cavarozzi, C., Maggi, J., 2005. Exhalación hidrotermal asociada al protolito de mármoles baritínicos de alto grado en las Sierras Pampeanas de San Luis. 16° Congreso Geológico Argentino 1, 33-40.

González, P.D., Sato, A., Llambías, E., 2006. Deformación y edad de plutones y diques monzonítico graníticos post-orogénicos tempranos del oeste de la Sierra de San Luis. In: Aceñolaza, F. (Ed.), Temas de la Geología Argentina I, San Miguel de Tucumán. INSUGEO, Serie Correlación Geológica 21, 105-132.

Graf, Jr., J., 1978. Rare earth elements, iron formations and sea water. Geochimica et Cosmochimica Acta 42, 1845-1850.

Gromet, P., Dymek, R., Haskin L., Korotev, R., 1984. The "North American Shale Composite": its compilation, major and trace element characteristics. Geochimica et Cosmochimica Acta 48, 2469-2482.

Gross, G., 1980. A classification of iron-formation based on depositional environments. Canadian Mineralogist 18 (2), 215-222.

Gross, G., 1996. Algoma-type Iron-Formation. In: Lefebure, D., Hõy, T. (Eds.), Selected British Columbia Mineral Deposits Profiles. British Columbia Ministry of Employment and Investment, Ottawa, Open File 1996-13 (2), pp. 25-28.

Haase, C., 1982. Metamorphic petrology of the Negaunee Iron Formation, Marquette district, northern Michigan: Mineralogy, metamorphic reactions and phase equilibria. Economic Geology 77, 60-81.

Hatton, O., Davidson, G., 2004. Soldiers Cap Group iron-formations, Mt. Isa Inlier, Australia, as windows into the hydrothermal evolution of a base-metal-bearing Proterozoic rift basin. Australian Journal of Earth Sciences 51, 85-106.

Hamade, T., Konhauser, K., Raiswell, R., Goldsmith, S., Morris, R., 2003. Using Ge/Si ratio to decouple iron and silica fluxes in Precambrian banded iron formations. Geology 31 (1), 35-38.

Henderson, P., 1984. General geochemical properties and abundances of the Rare Earth Elements. In: Henderson, P. (Ed.), Rare Earth Element Geochemistry, Developments in Geochemistry 2. Elsevier, Amsterdam, pp. 1-32.

Höll, R., Kling, M., Schroll, E., 2007. Metallogenesis of germanium-A review. Ore Geology Review 30 (3-4), 145-180.

Horstmann, U., Hälbich, I., 1995. Chemical composition of banded iron formations of the Griqualand West Sequence, Northern Cape Province, South Africa, in comparison with other Precambrian iron formations. Precambrian Research 72, 109-145.

Huston, D., Logan, G., 2004. Barite, BIFs and bugs: evidence for the evolution of the Earth's early hydrosphere. Earth and Planetary Science Letters 220, 41-55.

Immega, I., Klein, C., 1976. Mineralogy and petrology of some metamorphic Precambrian iron-formations in southwestern Montana. American Mineralogist 61, 1117-1144.

Jacobsen, S., Pimentel-Klose, M., 1988. A Nd isotopic study of the Hamersley and Michipicoten banded iron formations: the source of REE and Fe in Archean oceans. Earth and Planetary Science Letters 87 (1-2), 29-44.

James, H., 1954. Sedimentary facies of iron-formation. Economic Geology 49, 235-293.

James, H., 1966. Chemistry of the iron-rich sedimentary rocks. U.S. Geological Survey, Professional Paper 440-W, 61 p.

James, H., 1983. Distribution of Banded Iron Formation in space and time. In: Trendall, A., Morris, R. (Eds.), Iron-Formation: Facts and Problems. Elsevier, Amsterdam, pp. 471-490.

James, H., Sims, P., 1973. Precambrian iron-formations of the world. Economic Geology 68 (7), 913-914.

Klein, C., 1973. Changes in mineral assemblages with metamorphism of some banded Precambrian iron-formations. Economic Geology 68 (7), 1075-1088.

Klein, C., 1978. Regional metamorphism of Proterozoic iron-formation, Labrador Trough, Canada. American Mineralogist 63, 898-912.

Klein, C., 1983. Diagenesis and metamorphism of Precambrian banded iron-formation. In: Trendall, A., Morris, R. (Eds.), Iron-Formation: Facts and Problems. Elsevier, Amsterdam, pp. 417-469.

Klein, C., Beukes, N., 1993. Sedimentology and geochemistry of the glaciogenic Rapitan iron-formation in Canada. Economic Geology 88, 542-565.

Klein, C., Ladeira, E., 2000. Geochemistry and petrology of some Proterozoic Banded Iron Formations of the Quadrilátero Ferrífero, Minas Gerais, Brazil. Economic Geology 95, 405-428.

Kretz, R., 1983. Symbols for rock-forming minerals. American Mineralogist 68, 277 - 279.

Lagoeiro, L., 1998. Transformation of magnetite to hematite and its influence on the dissolution of iron oxide minerals. Journal of Metamorphic Geology 16, 415-423.

Leake, B., Woolley, A., Arps, C., Birch, W., Gilbert, M., Grice, J., Hawthorne, F., Kato, A., Kisch, H., Krivovichev, V., Linthout, K., Laird, J,. Mandarino, J., Maresch, W., Nickel, E., Rock, N., Schumacher, J., Smith, D., Stephenson, N., Ungaretti, L., Whittaker E., Youzih, G., 1997. Nomenclature of amphiboles: report of the Subcommittee on Amphiboles of the International Mineralogical Association, Commission on New Minerals and Minerals Names. American Mineralogist 82, 1019-1037.

Lottermoster, B., Ashley, P., 2000. Geochemistry, petrology and origin of Neoproterozoic ironstones in the eastern part of the Adelaide Geosyncline, South Australia. Precambrian Research 101, 49-67.

Ludwig, K., 2001. Users manual for Isoplot/Ex 2.49. A geochronological toolkit for Microsoft Excel. Berkeley Geochronological Center, Special Publication 1a, pp. 1-55.

Llambías, E., Sato, A.M., Ortiz Suárez, A., Prozzi, C., 1998. The granitoids of the Sierra de San Luis. In: Pankhurst, R., Rapela, C. (Eds.), The Proto-Andean Margin of Gondwana. Geological Society of London, Special Publication 142, 325-341.

Manikyamba, C., Naqvi, S., 1995. Geochemistry of Fe-Mn formations of the Archaean Sandur schist belt, India - mixing of clastic and chemical processes at a shallow shelf. Precambrian Research 72, 69-95.

Mezger, K., Essene, E.J., Halliday, A.N., 1992. Closure temperatures of the Sm-Nd system in metamorphic garnets. Earth and Planetary Science Letters 113, 397-409.

Murray, R., Brink, M., Gerlach, D., Russ, G., Jones, D., 1991. Rare earth, major and trace elements in chert from the Franciscan complex and Monterey Group, California: Assessing REE sources to fine grained marine sediments. Geochimica et Cosmochimica Acta 55, 1875-1895.

Nakamura, N., 1974. Determination of REE, Ba, Fe, Mg, Na and K in carbonaceous and ordinary chondrites. Geochimica et Cosmochimica Acta 38, 757-775.

Ortiz Suárez, A., 1999. Geología y petrología del área de San Francisco del Monte de Oro, San Luis. Ph.D. Thesis (Unpublished). Facultad de Ciencias Físico Matemáticas y Naturales, Universidad Nacional de San Luis, pp. 256.

Passchier, C., Trouw, R., 1996. Microtectonics. Springer Verlag, Berlín, 325 p.

Ramos, V., 1988. Late Proterozoic-Early Paleozoic of South America-a collisional history. Episodes 11, 168-173.

Ramos, V., 1991. Los ambientes tectónicos de los distritos wolframíferos de las Sierras Pampeanas. In: Brodtkorb, M. (Ed.), Publicación del Instituto de Recursos Minerales (Universidad Nacional de La Plata) 1, 185-196.

Ramos, V., Vujovich, G., 1993a. Laurentia-Gondwana connection: a Southamerican perspective. Geological Society of America, Annual Meeting. Abstracts with Programs A-232.

Ramos, V., Vujovich, G., 1993b. Alternativas de la evolución del borde occidental de América del Sur durante el Proterozoico. Revista Brasileira de Geociéncias 23 (3), 194-200.

Ramos, V., Dallmeyer, R., Vujovich, G., 1998. Time constraints on the Early Paleozoic docking of the Precordillera, central Argentina. In: Pankhurst, R., Rapela, C. (Eds.), The Proto-Andean Margin of Gondwana. Geological Society of London, Special Publication 142, 143-158.

Rosière, C., Siemes, H., Quade, H., Brokmeier, H., Jansen, E., 2001. Microstructures, textures and deformation mechanism in hematite. Journal of Structural Geology 23, 1429-1440.

Sato, K., Tassinari, C.C.G., Kawashita, K., Petronilho, L., 1995. O método geocronológico Sm-Nd no IG/USP e suas aplicações. Anais da Academia Brasileira de Ciências 67, 313-336.

Sato, A., González, P.D., Sato, K., 2001a. First indication of Mesoproterozoic age from the western basement of Sierra de San Luis. 3º South American Symposium on Isotope Geology, Santiago, Chile, Extended Abstracts Volume, 241-244.

Sato, A.M., González, P.D., Petronilho, L.A., Llambías, E.J., Varela, R., Basei, M.A., 2001b. Sm-Nd, Rb-Sr and K-Ar age constraints of the El Molle and Barroso plutons, western Sierra de San Luis, Argentina. 3º South American Symposium on Isotope Geology, Santiago, Chile, Extended Abstract Volume, 241-244.

Sato, A.M., González, P.D., Llambías, E., 2002. The Ordovician of Sierra de San Luis: Famatinian magmatic arc and low to high-grade metamorphism. In: Aceñolaza, F. (Ed.), Aspects on the Ordovician System of Argentina. Serie Correlación Geológica 16, INSUGEO, San Miguel de Tucumán, 327-346.

Sato, A., González, P.D, Llambias, E., 2003a. Evolución del orógeno Famatiniano en la Sierra de San Luis: magmatismo de arco, deformación y metamorfismo de bajo a alto grado. Revista de la Asociación Geológica Argentina 58 (4), 487-504.

Sato, A.M., González, P.D., Basei, M., Passarelli, C., Tickyj, H., Ponce, J., 2003b. The Famatinian granitoids of the southwestern Sierra de San Luis, Argentina. 4° South American Symposium on Isotope Geology 1, 290-293.

Sato, A.M., González, P.D., Basei, M.A., Passarelli, C.R., Petronilho, L.A., Sato, K., Vlach, S.R.F., Varela, R., Llambías, E., 2004. The Famatinian Orogeny of Western Sierra de San Luis, Argentina: Isotopic features. Simposio 40 Anos de Geocronología No Brasil. Boletim de Resumos, pp. 83.

Sato, A.M., Gonzalez, P.D., Basei, M.A., 2005. Los ortogneises granodioríticos del Complejo Metamórfico Nogolí, Sierra de San Luis. 16° Congreso Geológico Argentino 1, 41-48.

Sato, A.M, González, P.D., Basei, M.A., Llambías, E., 2006. U-Pb ages of komatiitic rocks from Sierra de San Luis, Argentina. 5º South American Symposium on Isotope Geology, Punta del Este, Uruguay, Short Papers Volume, 169-173.

Sharp, Z., 1991. Determination of oxygen diffusion rates in magnetite from natural isotopic variations. Geology 19, 653-656.

Sims, J., Ireland, T., Camacho A., Lyons, P., Pieters, P., Skirrow, R., Stuart Smith P., Miró, R., 1998. U-Pb, Th-Pb and Ar-Ar geocronology from the southern Sierras Pampeanas, Argentina: implications for the Paleozoic tectonic evolution of the western Gondwana margin. In:

Pankhurst, R., Rapela, C. (Eds.), The Proto-Andean Margin of Gondwana. Geological Society of London, Special Publications 142, 259-281.

Smulikowski, W., Desmons, J., Fettes, D., Harte, B., Sassi F., Schmidt, R., 2004. A systematic nomenclature for metamorphic rocks: 2. Types, Grade and Facies of Metamorphism. Recommendations by the IUGS Subcommission on the S.M.R. http://www.bgs.ac.uk/SCMR/

Spear, F., 1993. Metamorphic phase equilibria and pressure-temperature-time paths. Mineralogical Society of America, Washington, D.C., 799 p.

Thöni, M., 2003. Sm-Nd isotope systematics in garnet from different lithologies (Eastern Alps): age results, and an evaluation of potential problems for garnet Sm-Nd chronometry. Chemical Geology 194, 353-379.

Tracy, R., Frost, B., 1991. Phase equilibria and thermobarometry of calcareous, ultramafic and mafic rocks, and iron-formations. In: Ribbe, P. (Ed.), Contact Metamorphism. Book Crafters, Michigan. Reviews in Mineralogy 26, pp 207-289.

Trendall, A., 1965. Progress report on the Brockman Iron Formation in the Wittenoom-Yampire area. Western Australia Geological Survey, Annual Report 1964, 55-65.

Trendall, A., 1983. The Hamersley Basin. In: Trendall, A., Morris, R. (Eds.), Iron-Formation: Facts and Problems. Elsevier, Amsterdam, pp. 69-129.

Tsikos, H., Moore, J., 1997. Petrology and geochemistry of the Paleoproterozoic Hotazel Iron Formation, Kalahari Manganese Field, South Africa: implications for Precambrian Manganese Metallogenesis. Economic Geology 92, 87-97.

Unrug, R., 1996. The assembly of Gondwanaland. Episodes 19 (1-2), 11-20.

von Gosen, W., Prozzi, C., 1998. Structural evolution of the Sierra de San Luis (Eastern Sierras Pampeanas, Argentina): implications for the Proto-Andean Margin of Gondwana. In: Pankhurst, R. Rapela, C. (Eds.), The Proto-Andean Margin of Gondwana. Geological Society of London, Special Publications 142, 235-258.

von Gosen, W., Loske W., Prozzi, C., 2002. New isotopic dating of intrusive rocks in the Sierra de San Luis (Argentina): implications for the geodynamic history of the Eastern Sierras Pampeanas. Journal of South American Earth Sciences 15, 237-250.

Vujovich, G., Ostera, H., 2003. Evidencias del ciclo Pampeano en el basamento del sector noroccidental de la Sierra de San Luis. Revista de la Asociación Geológica Argentina 58 (4), 541-548.

Wonder, J., Spry, P., Windom, K., 1988. Geochemistry and origin of manganese-rich rocks related to iro-formation and sulfide deposits, western Georgia. Economic Geology 83 (5), 1070-1081.

Yardley, B., 1989. An introduction to Metamorphic Petrology. Longman Scientific & Technical, Harlow, UK, 248 p.

Figure Captions

Fig. 1. Simplified geological map of the banded iron formation from the Nogolí Metamorphic Complex of western Sierra de San Luis (Nogolí area), Eastern Sierras Pampeanas of Argentina (adapted after González, 2003).

Fig. 2. Detailed geological map of the largest bed of the banded iron formation, showing location of samples cited in the text. See Fig. 1 for location of map.

Fig. 3. (a) to (d). Polished hand specimen of the banded iron formation showing the fine- to medium-grained laminae and bands composed of variable amounts of iron oxides (mainly magnetite), minor hydroxides, iron and magnesium silicates, and quartz. The lamination and banding reflect the primary layering S_0 of the protolith.

Fig. 4. Lower hemisphere, equal area stereographic projections of fabric elements from the banded iron formation and its country rocks.

Fig. 5. Photomicrographs from thin sections showing the mineralogy and textural arrangement of seven types of laminae-bands from the banded iron formation. (a). Type 1: magnetite-rich laminae-bands. (b). Type 2: quartz-rich laminae-bands. (c). Type 3: poikiloblastic garnet-rich laminae-bands. (d). Type 4: details of garnets with magnetite inclusions arranged in concentric shells. (e). Type 5: massive garnet aggregates. (f). Type 6: polygonal granoblastic garnet with intercalations of apatite lenses (this last mineral is not shown here). (g). Type 6: details of apatite lenses. (h). Type 7: amphibole-rich laminae-bands. Mineral abbreviations after Kretz (1983). Transmitted light, parallel nicols. See details discussed in text.

Fig. 6. Compositional diagrams of (a) amphibole (after Leake et al. 1997) and (b) garnets, performed with selected electron microprobe analyses given in Table 2 (sample Fe-5) and unpublished data (samples NG-29 and Fe-1) from González (2003).

Fig. 7. Photomicrographs from thin sections showing mineral assemblages and microfabrics of the banded iron formation. (a) and (b). Greenschist facies M_1 assemblage. (c). Amphibolite facies M_2 assemblage. (d) and (e). Amphibolite facies M_4 garnets. (f). Apatite and garnet showing interlobate to amoeboid grain boundaries. (g) and (h). Relict grains of greenalite - iron oxide/hydroxide in magnetite. Mineral abbreviations after Kretz (1983). Transmitted light, parallel nicols (only (b) with crossed nicols). See details discussed in text.

Fig. 8. Photomicrographs from thin sections showing some details of mineral assemblages and microfabrics of the banded iron formation. (a). Peak M_4-D_4 assemblage with garnet. (b) and (c). Retrograde greenschist facies M_5 assemblage with epidote. (d). Contact metamorphism. Mineral abbreviations after Kretz (1983). Transmitted light, parallel nicols.

Fig. 9. Photomicrographs from thin sections. (a) and (c). Complex inclusion trails of quartz, apatite and magnetite in large intertectonic (post D_{1-2} and pre- to syn-D_4) garnet poikiloblasts. (b) and (d). Line drawing from pictures (a) and (c) respectively. (e). Possible polygonal arcs of recrystallized quartz + magnetite + cummingtonite. (f). Isoclinal F_1 micro-fold of primary lamination S_0. (g). Micro-boudin in granoblastic garnet aggregate. Mineral abbreviations after Kretz (1983). Transmitted light, parallel nicols in (a), (c), (f) and (g). Crossed nicols in (e).

Fig. 10. *P-T* diagram of the San Luis banded iron formation based on mineral assemblages, textural analyses, and electron probe micro-analytical data of amphiboles and garnets. The broadly estimated *P-T* conditions show a clockwise metamorphic evolution with three distinctive trajectories: (1) Relict prograde M_1-M_3 segment (subgreenschist facies at M_1 to amphibolite facies at M_3). (2) Peak at high amphibolite-low granulite facies during M_4. (3) Retrograde counterpart of M_4, stabilized at greenschist facies during M_5.

Fig. 11. (a). Diagram after Wonder et al. (1988) to illustrate the primary chemical precipitation of the San Luis BIF from seawater, based on Al_2O_3-SiO_2 contents. (b). Fe/Ti – Al/(Al+Fe+Mn) discrimination diagram (after Bostrom, 1973) showing the hydrothermal input and volcanic-clastic

components in the hydrogenous sediment. The well-known hydrothermal chemical sediment of the Soldier Cap Group iron formations (after Hatton and Davidson, 2004) is plotted here (grey field) to show the hydrothermal input into the San Luis BIF. NMC=Nogolí Metamorphic Complex.

Fig. 12. (a) to (g). Inter-element scatter diagrams from San Luis banded iron formation used as clues suggesting both, the hydrothermal fluids input and the influence of volcanic and clastic components into the primary chemical sediment. Arrows indicate the positive inter-element correlations. (h). Some metal contents (ppm) in San Luis banded iron formation (black squares) compared with those from classical *Algoma*- (white squares) and *Lake Superior* Type trends (white diamonds).

Fig. 13. Shale-normalized REE plots for the San Luis banded iron formation. Normalized to NASC (North American Shale Composite) after Gromet et al. (1984).

Fig. 14. Sm-Nd whole rock + garnet isochron diagrams of three samples from the banded iron formation. See Fig. 2 for samples locations.

Tables

Table 1. Sequence of deformation and metamorphic phases in the Nogolí Metamorphic Complex. Adapted after González et al. (2004).

	DEFORMATION	METAMORPHISM	AGE
PENETRATIVE NNE-SSW TO NE-SW FAMATINIAN FABRICS	D_5: ductile shear zones, mylonitic foliation S_5 and S-C fabric.	M_5: local retrograde amphibolite to greenschist facies.	445-364 Ma
	D_4: foliation S_4, stretching plus mineral lineation L_4 and tight to isoclinal folds F_4.	M_4: prograde regional medium *P* (Barrovian type) / high *T*, transitional between high amphibolite and granulite facies. (ca. 8 kb and 636° - 820°C).	475-457 Ma
RELICT W-E TO NW-SE PRE-FAMATINIAN FABRICS	D_3: mylonitic foliation S_3, stretching lineation L_3, injection of second generation of granitic veins accompanied by syn-tectonic intrusions of granitoid lenses. Final stage of open folds F_3.	M_3: peak *P-T* conditions at high amphibolite facies (<700°C)	Pre-507 Ma
	cm-thick ductile shear zones associated with mylonitic foliation S_3. Injection of second generation of granitic veins.		
	D_2: foliation S_2, stretching lineation L_2 and tight folds F_2.	M_2: middle amphibolite facies. (3 - 5 kb and 525° - 640°C)	
	D_1: injection of first generation of quartz-plagioclase (± biotite) veins, growth of muscovite flakes, axial plane foliation S_1 and isoclinal folds F_1.	M_1: prograde regional metamorphism from at least middle greenschist facies. (2 - 4 kb and 450° - 575°C)	
Pelitic and psammitic siliciclastic and mafic-ultramafic to felsic volcanic protoliths with interlayered oxide facies *Algoma type* iron formation and Ba-bearing exhalites.			ca. 1500 Ma

Table 2. Selected electron probe microanalyses of cummingtonites and garnets from sample Fe-5. Mg# = Mg/Mg + Fe^{2+} and Fe# = 1.0-Mg#. XFe = Fe^{2+} / Fe^{2+} + Mg. i. rim: inner rim.

	cummingtonites						garnets					
%	1	2	3	4	5		crystal 1			crystal 2		
SiO_2	52.110	51.355	51.339	51.662	51.958	%	i. rim	core	rim	i.rim	core	rim
TiO_2	0.000	0.000	0.011	0.048	0.000	**SiO_2**	36.527	36.563	36.809	36.741	36.748	36.858
Al_2O_3	0.678	0.428	0.737	0.521	0.397	**TiO_2**	0.000	0.015	0.000	0.001	0.026	0.026
FeO	27.802	27.104	27.373	27.521	26.346	**Al_2O_3**	20.845	20.887	20.835	20.901	20.758	21.375
MnO	0.832	0.775	0.813	0.801	0.795	**FeO**	33.721	33.449	33.642	33.699	33.888	34.228
MgO	15.769	15.730	15.638	15.579	16.284	**MnO**	5.539	5.485	5.404	5.426	5.458	5.420
CaO	0.091	0.027	0.062	0.041	0.028	**MgO**	2.762	2.775	2.775	2.726	2.862	2.616
Na_2O	0.020	0.008	0.013	0.009	0.018	**CaO**	1.162	1.283	1.142	1.031	0.975	0.613
K_2O	0.005	0.006	0.000	0.000	0.017	**Na_2O**	0.000	0.010	0.029	0.028	0.023	0.007
F	0.000	0.004	0.053	0.020	0.000	**K_2O**	0.000	0.003	0.000	0.005	0.000	0.000
Cl	0.000	0.003	0.012	0.000	0.000	**Total**	100.56	100.47	100.64	100.56	100.74	101.14
Total	97.31	95.44	96.05	96.20	95.84							
	cations per 23 oxygens						cations per 24 oxygens					
Si	7.8335	7.8598	7.8214	7.8541	7.8798	**Si**	5.9169	5.9204	5.9469	5.9415	5.9378	5.9240
Al^{IV}	0.1201	0.0772	0.1324	0.0983	0.0709	**Al^{IV}**	0.0831	0.0796	0.0531	0.0585	0.0622	0.0760
Sum T	7.9536	7.9370	7.9538	7.9524	7.9507	**Sum Z**	6.0000	6.0000	6.0000	6.0000	6.0000	6.0000
Al^{VI}	0.0000	0.0000	0.0000	0.0000	0.0000	**Al^{VI}**	3.8965	3.9065	3.9141	3.9250	3.8910	3.9730
Ti	0.0000	0.0000	0.0012	0.0054	0.0000	**Ti**	0.0000	0.0018	0.0000	0.0001	0.0032	0.0032
Mg	3.5339	3.5889	3.5516	3.5308	3.6817	**Sum Y**	3.8965	3.9083	3.9141	3.9251	3.8942	3.9762
Fe^{2+}	1.4661	1.4111	1.4472	1.4638	1.3183							
Sum C	5.0000	5.0000	5.0000	5.0000	5.0000	**Mg**	0.6669	0.6699	0.6684	0.6572	0.6895	0.6268
						Fe^{2+}	4.5682	4.5296	4.5454	4.5575	4.5793	4.6007
Fe^{2+}	2.0290	2.0580	2.0404	2.0352	2.0232	**Mn**	0.7599	0.7523	0.7394	0.7433	0.7470	0.7378
Mn	0.1060	0.1004	0.1032	0.1032	0.1022	**Ca**	0.2017	0.2226	0.1977	0.1787	0.1688	0.1056
Ca	0.0146	0.0044	0.0102	0.0067	0.0046	**Na**	0.0000	0.0032	0.0091	0.0089	0.0071	0.0023
Na	0.0000	0.0000	0.0000	0.0000	0.0000	**K**	0.0000	0.0006	0.0000	0.0010	0.0000	0.0000
Sum B	2.1496	2.1628	2.1538	2.1451	2.1300	**Sum X**	6.1967	6.1782	6.1600	6.1466	6.1917	6.0732
Na	0.0059	0.0024	0.0037	0.0026	0.0052	**Total**	16.093	16.086	16.074	16.071	16.085	16.049
K	0.0009	0.0011	0.0000	0.0000	0.0032							
Sum A	0.0068	0.0035	0.0037	0.0026	0.0084	**Pyrope**	0.1076	0.1085	0.1087	0.1071	0.1115	0.1032
						Alman	0.7372	0.7336	0.7390	0.7427	0.7404	0.7578
Total	15.1100	15.1033	15.1113	15.1001	15.0891	**Spess**	0.1226	0.1218	0.1202	0.1211	0.1208	0.1215
Mg#	0.5028	0.5085	0.5045	0.5023	0.5242	**Gros**	0.0325	0.0361	0.0321	0.0291	0.0273	0.0174
Fe#	0.4972	0.4915	0.4955	0.4977	0.4758	**XFe**	0.8726	0.8711	0.8718	0.8739	0.8691	0.8801

Table 3. Relationships between growth periods of metamorphic minerals and deformation phases. * Clinoamphibole$_2$ = cummingtonite.

	RELICT FABRICS			PENETRATIVE FABRICS		
DEFORMATION PHASE	**D_1** schistosity	**D_2** axial plane foliation	**D_3** mylonitic foliation	**D_4** foliation	emplacement of Barroso pluton	**D_5** mylonitic foliation
METAMORPHISM	**M_1** greenschist facies	**M_2** middle amphibolite facies	**M_3** upper amphibolite facies	**M_4** upper amphibolite facies	**CONTACT** hornblendic hornfels facies	**M_5** retrograde amphibolite to greenschist facies
QUARTZ						
BIOTITE						
CHLORITE						
GREENALITE						
Fe OXIDES-HYDROXIDES	? ? ? ?					
MAGNETITE						
GARNET				Xalm 0.73 - 0.75		
CLINOAMPHIBOLE		cu-gr$_1$	cu-gr$_1$	*XFe 0.47 – 0.49		
APATITE						
RUTILE			?			
PYRITE			? ? ?			
EPIDOTE						
ANTHOPHYLLITE						
CROCIDOLITE						
MINNESOTAITE						
HEMATITE (martite)						

Table 4. Major (wt.%), trace and REE (ppm, except Au in ppb) selected analyses from oxide facies iron formations of Nogolí Metamorphic Complex from western Sierra de San Luis. Fe# = FeO/FeO+MgO. Ca# = CaO/CaO+MgO. SN: shale normalized (NASC, Gromet et al., 1984). CN: chondrite normalized (Nakamura, 1974). $(Eu/Eu^*)_{SN}$ and $(Ce/Ce^*)_{SN}$ calculated according Bau and Dulski (1996). * All Fe as Fe^{3+}. (-) Not determined.

	NG 29	FE-1	FE-3	FE-4	FE-5
SiO_2	37.02	31.26	41.94	30.83	33.87
Al_2O_3	7.70	4.62	8.39	3.27	5.80
Fe_2O_3*	43.56	51.61	42.70	54.50	49.51
MnO	2.28	1.34	2.00	2.34	1.52
MgO	1.06	0.57	0.73	1.80	3.15
CaO	4.40	4.67	1.08	3.56	2.13
Na_2O	0.02	0.01	0.03	0.01	0.05
K_2O	0.06	0.17	0.07	0.01	0.01
TiO_2	0.28	0.14	0.28	0.13	0.17
P_2O_5	2.81	2.76	2.20	2.98	2.44
LOI	0.50	1.35	0.88	0.16	0.03
Total	99.71	98.50	100.30	99.23	98.68
V	288.00	227.41	202.19	232.80	167.87
Cr	77.00	48.33	70.00	49.19	58.88
Co	21.00	22.60	26.26	31.83	45.81
Ni	38.00	20.00	20.00	20.00	20.00
Cu	278.00	56.74	393.16	405.00	76.18
Zn	139.00	30.00	55.03	214.64	297.11
Ga	25.00	17.81	19.25	16.81	12.37
Ge	6.50	7.54	5.39	6.80	6.92
As	5.00	1.70	37.60	37.38	8.50
Rb	3.00	3.31	1.88	1.00	1.00
Sr	46.00	127.18	140.84	92.08	41.58
Ba	125.00	73.55	70.84	43.84	61.73
Y	36.20	30.49	42.23	45.77	23.95
Zr	68.00	37.62	66.78	28.70	41.50
Sc	6.00	4.50	9.00	3.00	6.00
Nb	4.60	1.63	5.90	3.68	2.27
Mo	4.00	2.66	6.46	2.58	2.91
Ag	0.50	0.50	0.50	0.50	0.50
Au (ppb)	-	290.00	247.00	-	268.00
In	3.20	1.24	1.21	3.55	2.36
Sn	72.00	17.59	28.13	158.76	58.09
Sb	0.20	0.45	0.10	0.32	0.20
Cs	0.10	0.24	0.23	0.10	0.10
La	21.40	24.61	31.30	24.14	15.85
Ce	34.70	38.96	46.77	28.08	23.94
Pr	4.71	4.60	8.04	5.11	3.06
Nd	18.80	19.82	27.77	21.07	12.44
Sm	4.03	4.06	5.83	4.65	2.63
Eu	1.44	1.99	1.51	1.94	0.71
Gd	4.40	3.98	6.40	5.55	2.77
Tb	0.78	0.67	1.15	1.01	0.48
Dy	4.79	4.07	7.24	6.25	2.97
Ho	1.00	0.82	1.60	1.34	0.65
Er	3.14	2.52	4.63	4.07	2.17
Tm	0.49	0.37	0.68	0.60	0.32
Yb	2.97	2.36	4.12	3.63	1.99
Lu	0.45	0.35	0.63	0.51	0.30
Hf	1.80	0.98	1.75	0.75	1.04
Ta	1.40	1.31	1.59	0.68	1.09
Tl	0.05	0.05	0.19	0.05	0.05
Pb	5.00	5.00	17.99	23.56	5.00
Bi	10.60	0.10	8.20	46.10	21.04
Th	5.57	4.40	7.20	3.23	4.54
U	3.69	2.75	5.40	2.70	1.81

Fe#	0.97	0.92	0.98	0.96	0.93
Ca#	0.81	0.89	0.60	0.66	0.40
$(Eu/Eu^*)_{SN}$	1.52	2.22	1.10	1.70	1.19
$(Ce/Ce^*)_{SN}$	0.81	0.85	0.69	0.59	0.80
$(Sm/Yb)_{SN}$	0.70	0.89	0.74	0.67	0.69
$(Eu/Sm)_{SN}$	1.71	2.34	1.24	1.99	1.29
$(La/Yb)_{SN}$	0.72	1.04	0.76	0.67	0.80
$(La/Sm)_{CN}$	0.63	0.72	0.64	0.62	0.72
$(Eu/Eu^*)_{CN}$	1.85	2.85	1.33	1.99	1.48

Table 5. Analytical results of Sm-Nd datings from the oxide facies iron formation. T_{DM} model ages calculated according to the model of De Paolo et al. (1991).

Sample	Material	Sm (ppm)	Nd (ppm)	$^{147}Sm/^{144}Nd$	$^{143}Nd/^{144}Nd$	T_{DM} (Ma)	$\xi Nd_{(1502)}$
Fe-1	whole rock	4.461	21.595	0.1249 ± 0.0004	0.512127 ± 0.000010	1670	+3.8
Fe-1	garnet	3.391	14.132	0.1451 ± 0.0006	0.512143 ± 0.000010		
Fe-3	whole rock	5.831	26.968	0.1307 ± 0.0004	0.512069 ± 0.000012	1854	+1.5
Fe-3	garnet	2.331	6.883	0.2048 ± 0.0008	0.512258 ± 0.000011		
Fe-5	whole rock	2.763	12.297	0.1359 ± 0.0005	0.512064 ± 0.000014	1939	+0.5
Fe-5	garnet	1.828	6.089	0.1815 ± 0.0007	0.512198 ± 0.000068		

Table 6. T_{DM} model ages of mafic to ultramafic metavolcanic rocks of Nogolí Metamorphic Complex calculated according to the model of De Paolo et al. (1991). Original data were taken from Sato et al. (2001a).

Sample	Rock Type	T_{DM} (Ma)	$\xi Nd_{(1502)}$
RQ-25-1	Komatiite	1679	+ 3.68
RQ-25-3	Amphibolite	1731	+ 3.06
SL-16-A	Amphibolite	1710	+ 3.31
RQ-16-1	Amphibolite	1718	+ 3.22
PN-22	Komatiite	1765	+ 2.64
VQ-101-2	Amphibolite	1733	+ 3.03
RQ-7-2	Amphibolite	1717	+ 3.24

Figure 1

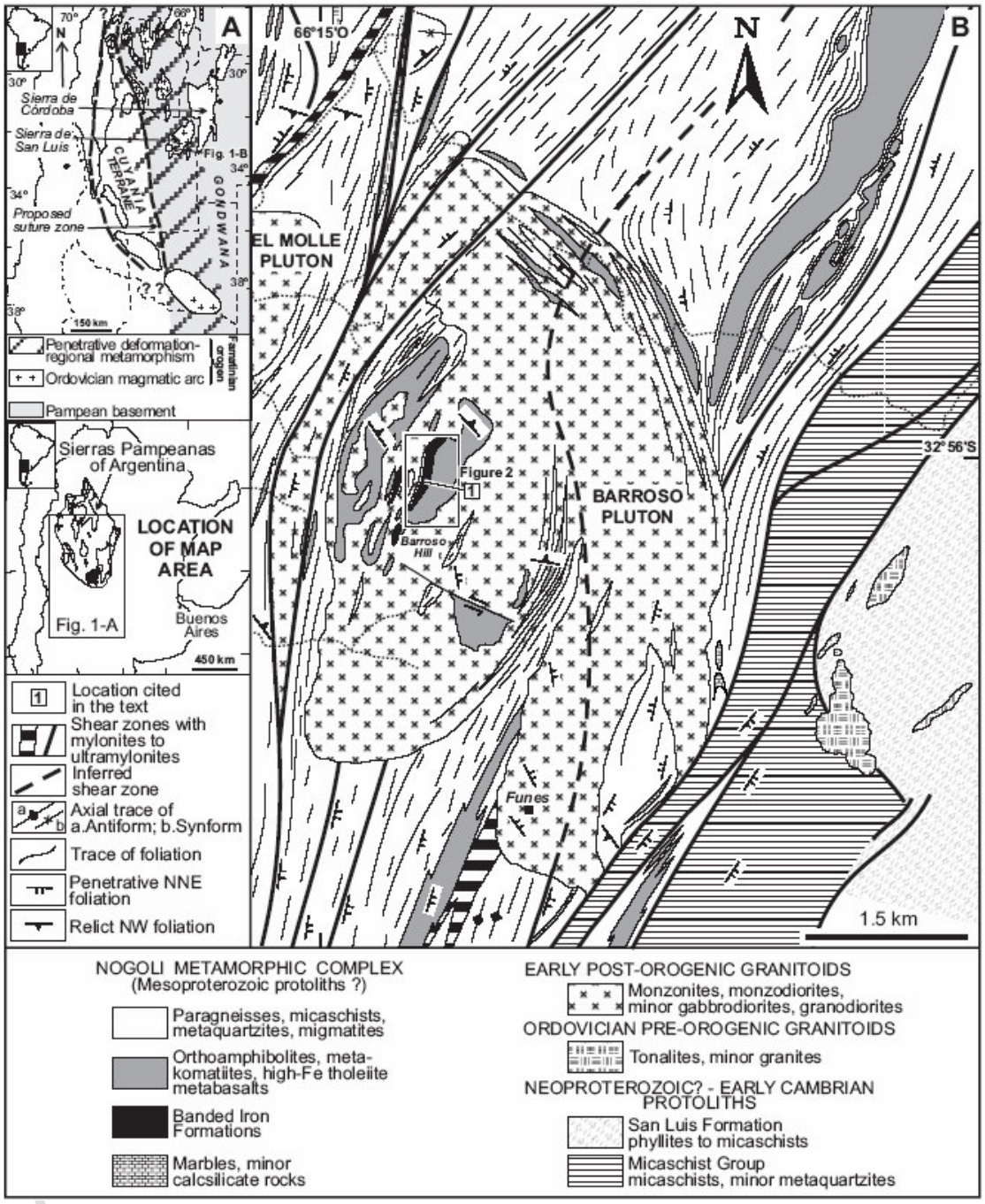

Figure 2

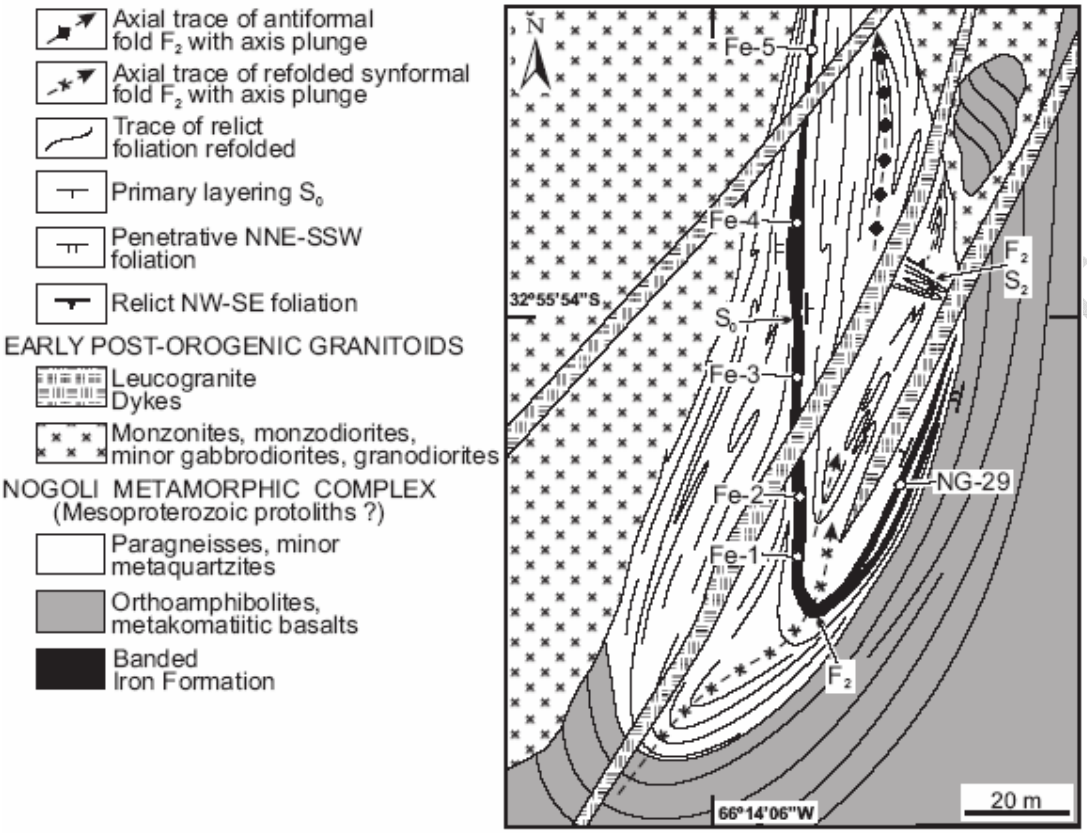

Figure 3

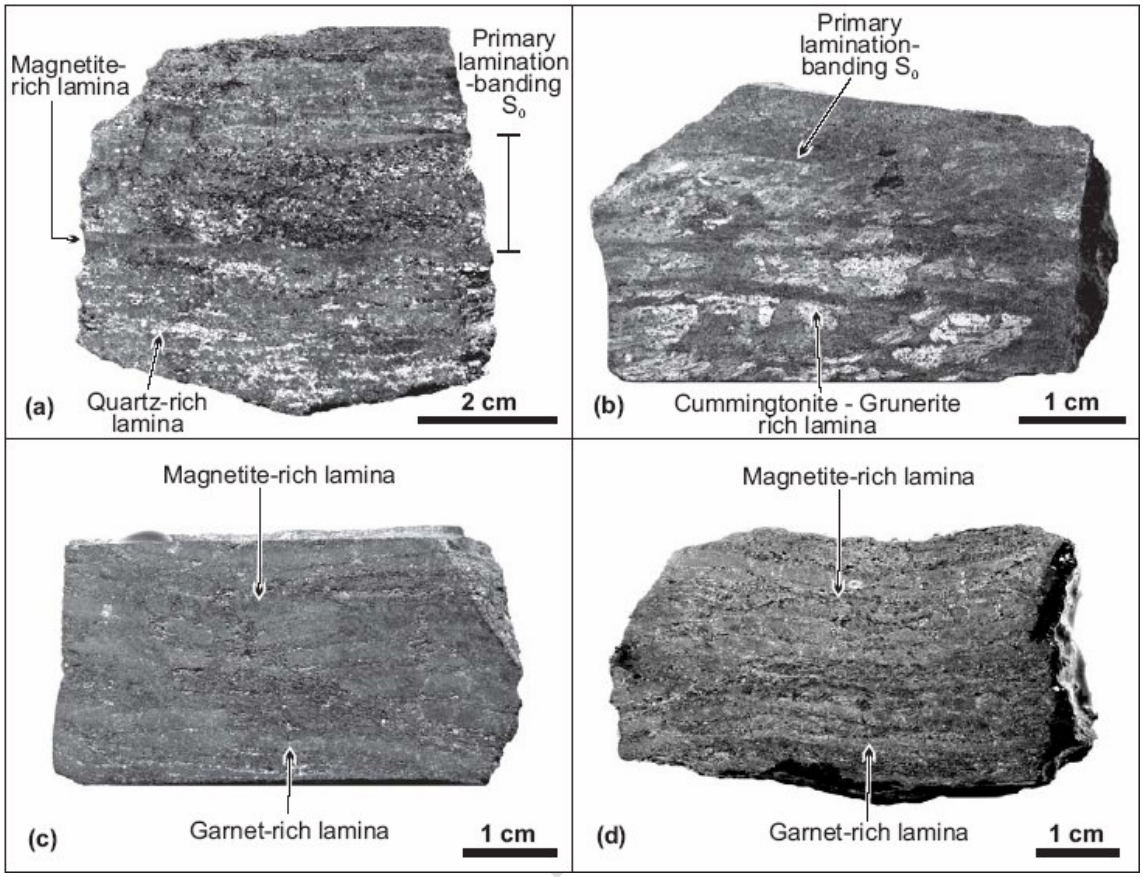

Figure 4

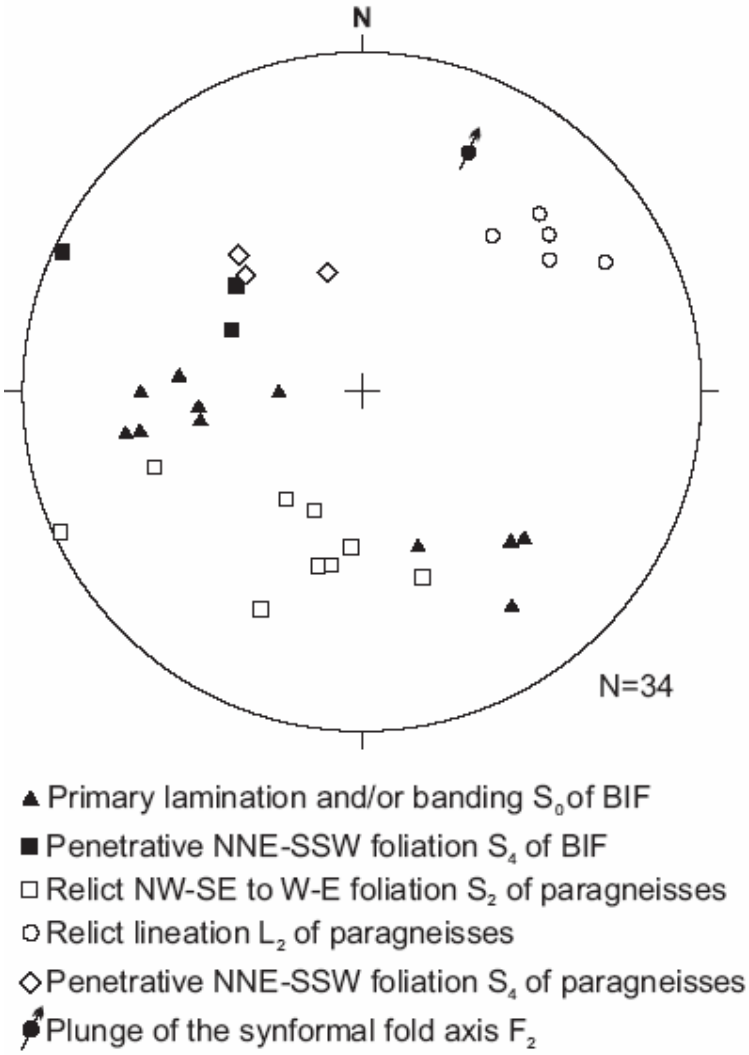

Figure 5

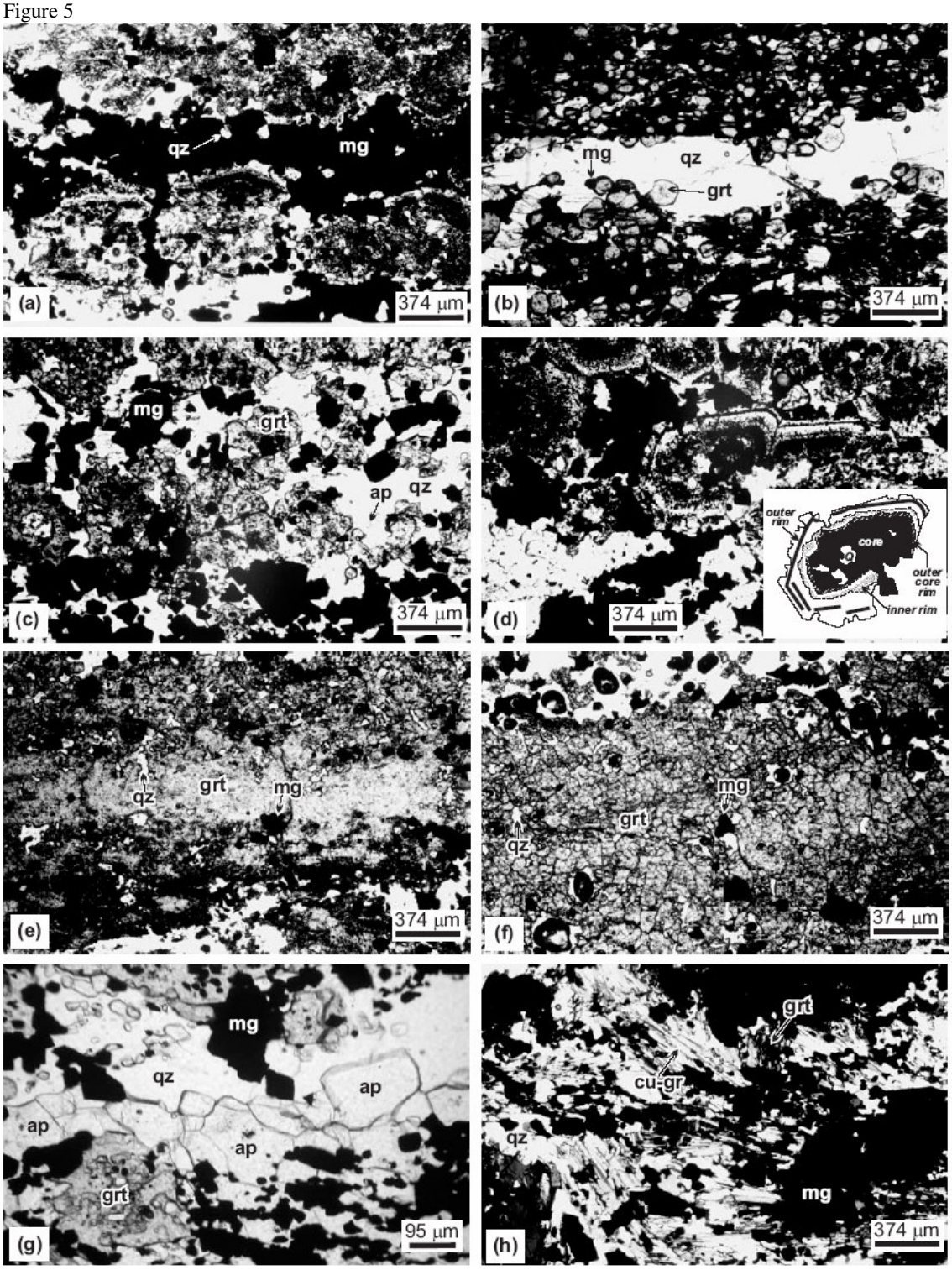

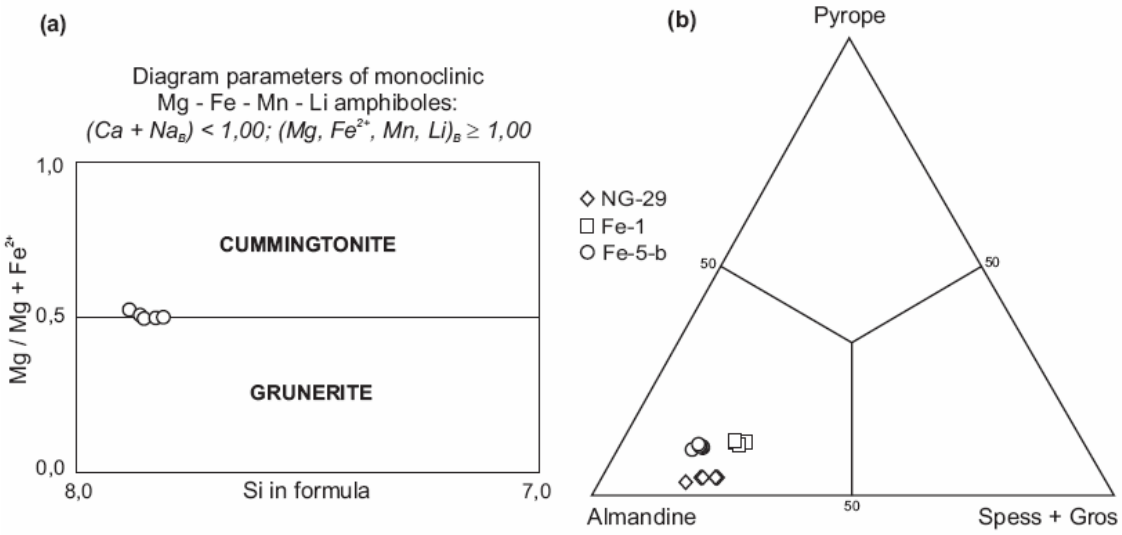

Figure 6

Figure 7

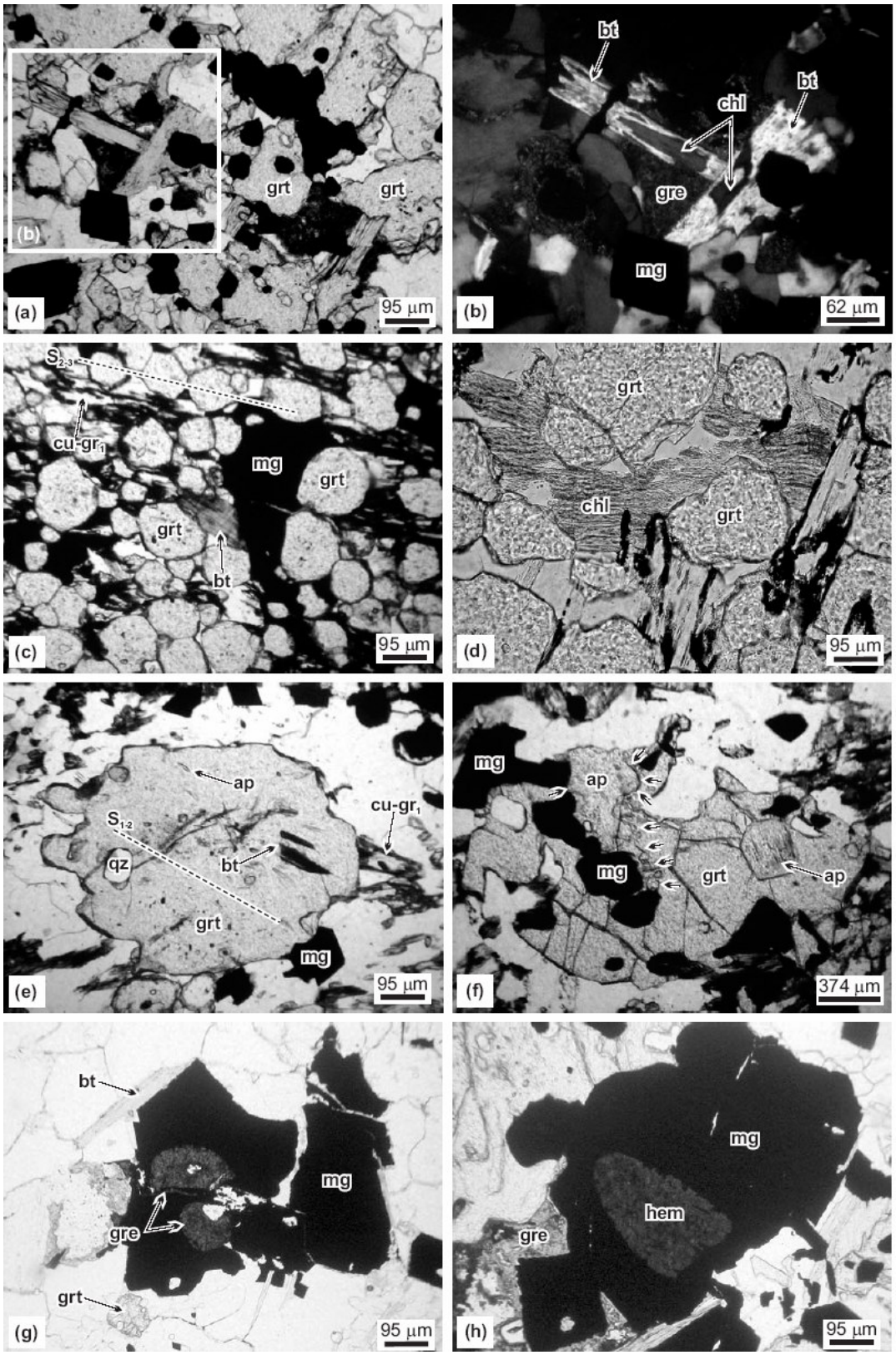

Figure 8

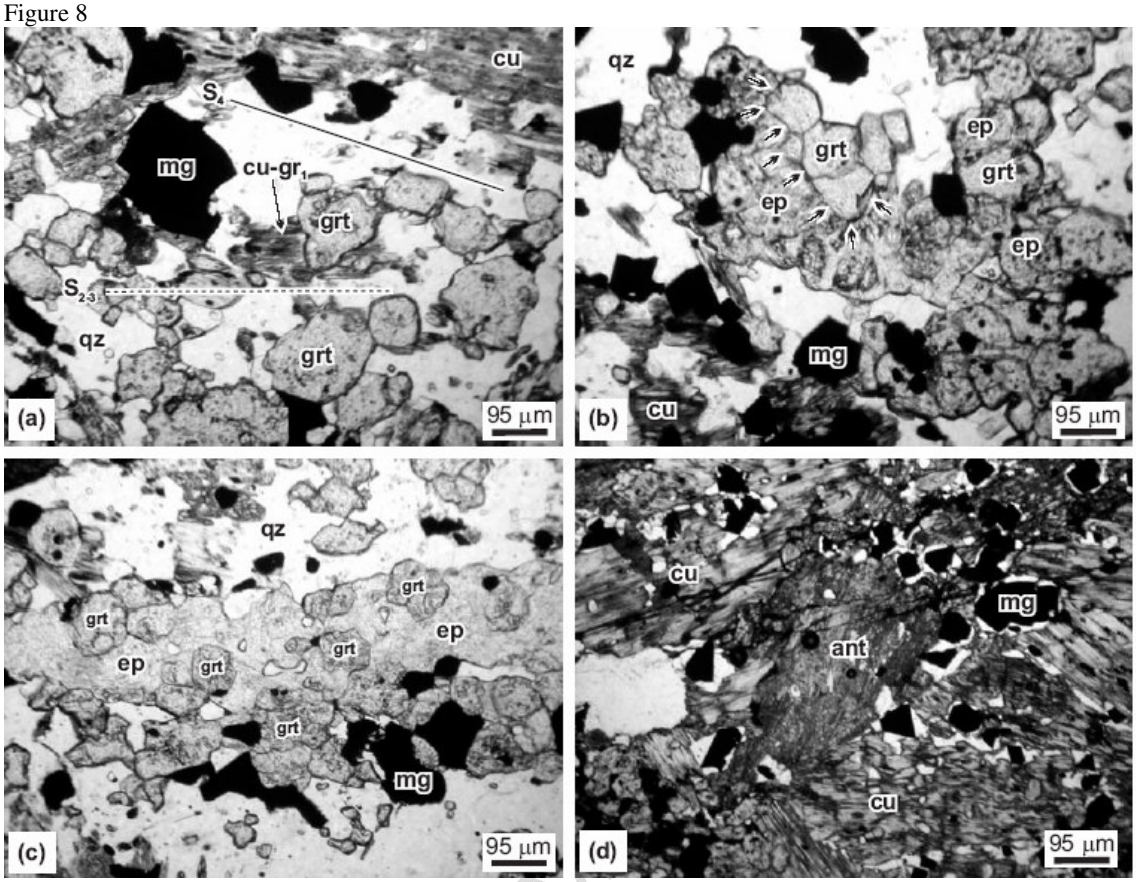

Figure 9

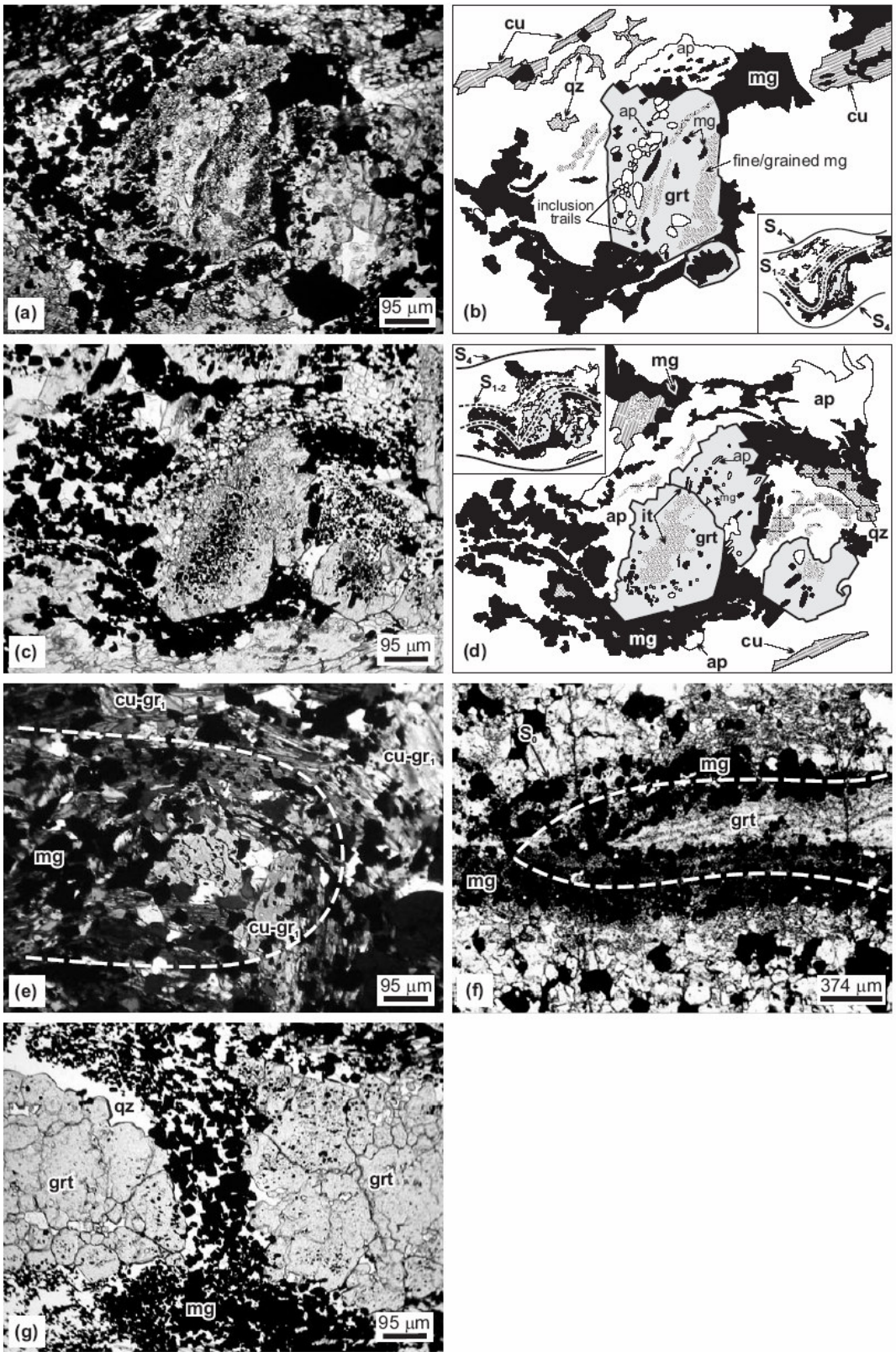

Figure 10

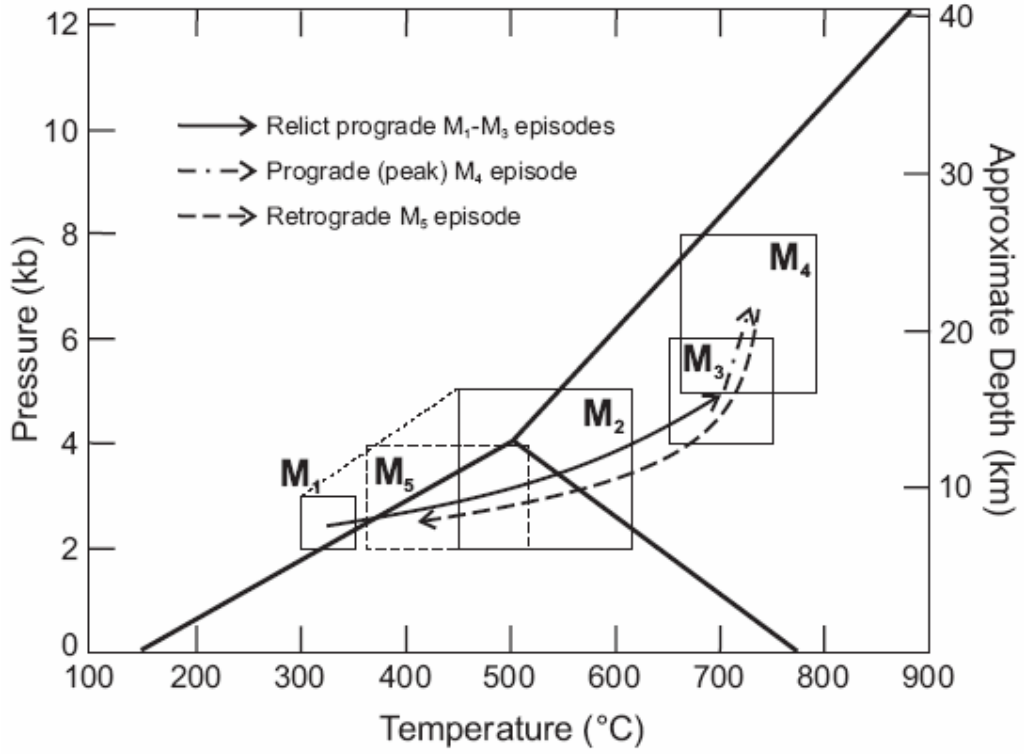

Figure 11

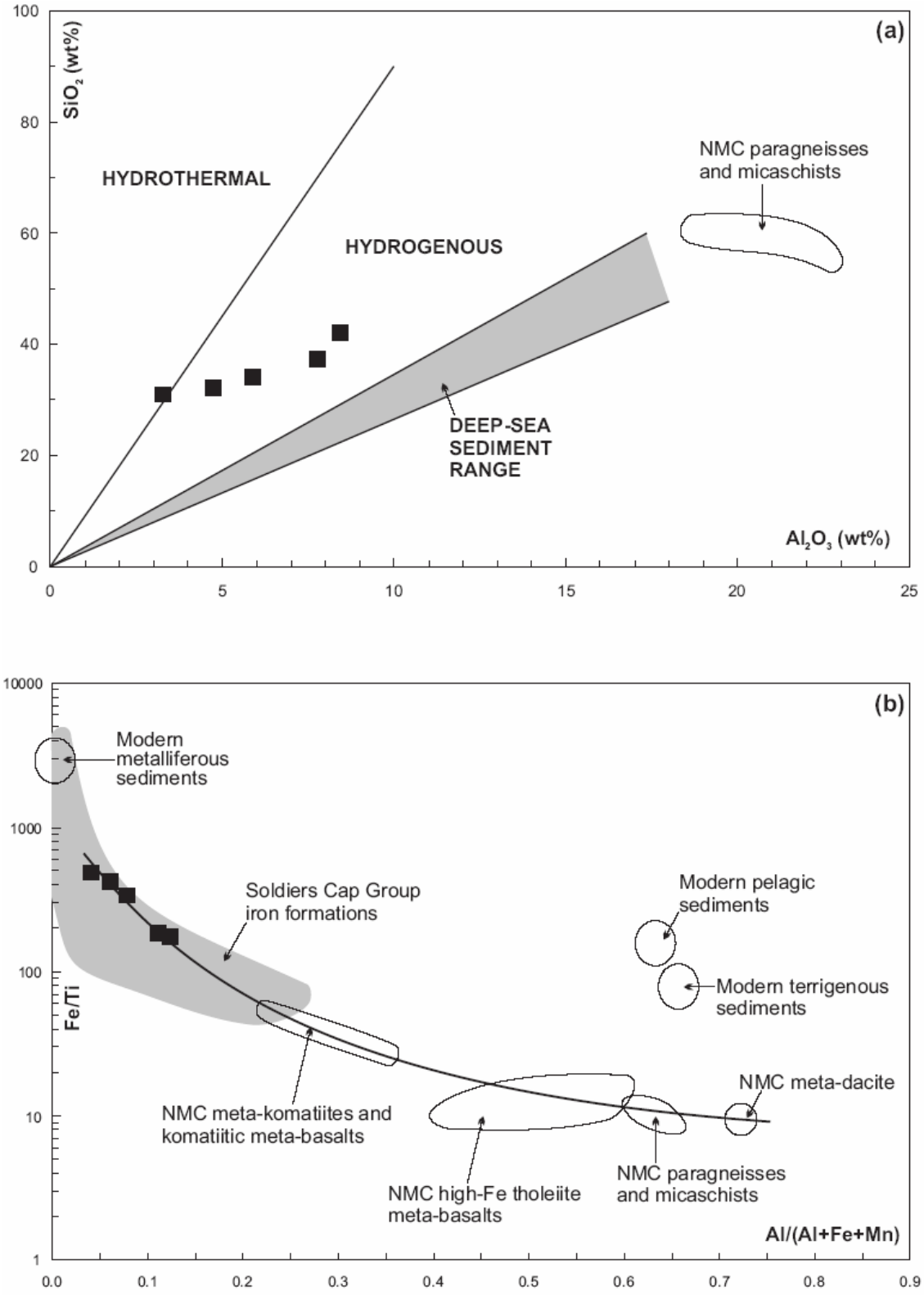

Figure 12

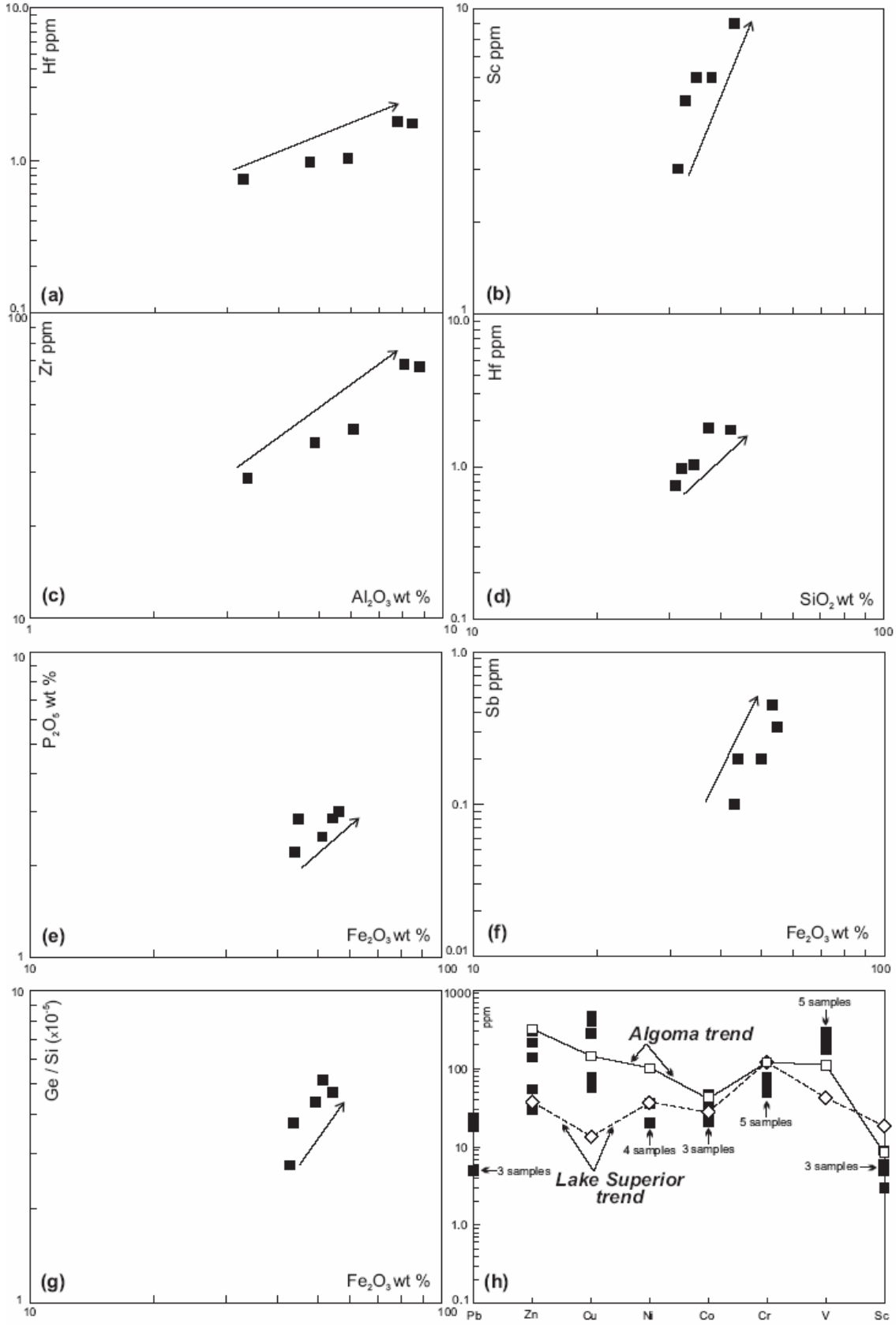

Figure 13

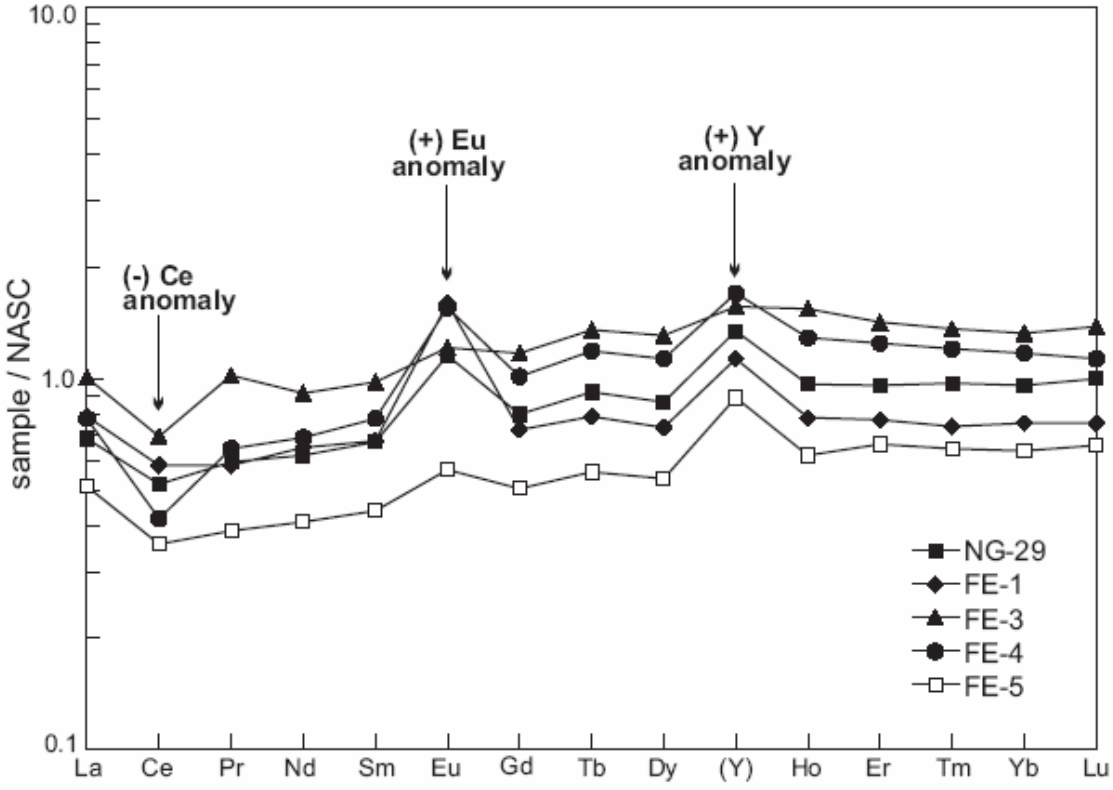

Figure 14